
SITE-SPECIFIC SEISMIC HAZARD EVALUATION OF THE LAKE ROBERTS DAM, NEW MEXICO



Prepared for
U.S. Fish and Wildlife Service

Prepared by
Ivan Wong, Patricia Thomas, Susan Olig, and Fabia Terra

URS
URS Corporation
Seismic Hazards Group
1333 Broadway, Suite 800
Oakland, CA 94612

22 November 2011

TABLE OF CONTENTS

Section 1	Introduction.....	1-1
	1.1 Scope of Work	1-1
	1.2 Acknowledgments.....	1-2
Section 2	Seismic Hazard Analysis Methodology	2-1
	2.1 Seismic Source Characterization	2-2
	2.2 Ground Motion Prediction Models	2-4
Section 3	Seismotectonic Setting and Historical Seismicity.....	3-1
	3.1 Seismotectonic Setting.....	3-1
	3.2 Historical Seismicity.....	3-1
Section 4	Probabilistic Seismic Hazard Analysis Input	4-1
	4.1 Earthquake Sources.....	4-1
	4.1.1 Quaternary Faults.....	4-1
	4.1.2 Background Seismicity	4-4
	4.2 Ground Motion Prediction Models	4-5
Section 5	Seismic Hazard Results	5-1
	5.1 Hazard Results	5-1
	5.2 Comparison With the USGS National Hazard Maps.....	5-1
	5.3 Comparison With Deterministic Hazard Analysis.....	5-2
Section 6	References	6-1

Tables

1	Fault Source Parameters for Lake Roberts Dam Analysis
2a	Southern California and Baja California Fault Source Parameters
2b	Maximum Magnitudes and Rupture Rates for the Southern San Andreas Fault
2c	Maximum Magnitudes and Rupture Rates for the San Jacinto Fault
2d	Maximum Magnitudes and Rupture Rates for the Elsinore Fault
3	UHS
4	PSHA Deaggregation
5	DSHA Results

Figures

1	Tectonic Setting of Lake Roberts Dam
2	Historical Seismicity in the Site Region (1938 to 2010)

TABLE OF CONTENTS

3	Quaternary Faults in the Site Region
4	Isoseismal Map of 3 May 1887 M 7.4 Sonora, Mexico Earthquake
5	Seismic Hazard Model Logic Tree
6	Seismic Hazard Curves for Peak Horizontal Acceleration
7	Seismic Hazard Curves for 1.0 Sec Horizontal Spectral Acceleration
8	Seismic Source Contributions to Mean Peak Horizontal Acceleration Hazard
9	Seismic Source Contributions to Mean 1.0 Sec Horizontal Spectral Acceleration Hazard
10	Magnitude and Distance Contributions to the Mean Peak Horizontal Acceleration Hazard at 2,475-Year Return Period
11	Magnitude and Distance Contributions to the Mean Peak Horizontal Acceleration Hazard at 10,000-Year Return Period
12	Magnitude and Distance Contributions to the Mean 1.0 Sec Horizontal Spectral Acceleration Hazard at 2,475-Year Return Period and 0 to 100 km
13	Magnitude and Distance Contributions to the Mean 1.0 Sec Horizontal Spectral Acceleration Hazard at 10,000-Year Return Period
14	Sensitivity of the Peak Horizontal Acceleration Hazard to the Selection of Ground Motion Prediction Models
15	Sensitivity of the Peak 1.0 Sec Horizontal Spectral Acceleration Hazard to the Selection of Ground Motion Prediction Models
16	5%-Damped Uniform Hazard Spectra at 2,475 and 10,000-Year Return Periods
17	5%-Damped Uniform Hazard Spectra at 2,475, 5,000, and 10,000-Year Return Periods
18	84th Percentile Horizontal Acceleration Response Spectra for the M 6.9 Mockingbird Hill/Mogollon Fault Maximum Earthquake
19	5%-Damped Uniform Hazard Spectrum Compared to 84th Percentile Deterministic Spectra for Mockingbird Hill/Mogollon Fault

Lake Roberts Dam is located in Grant County in southwestern New Mexico (Figure 1). Tectonically the damsite is within the Southern Basin and Range Province and the Rio Grande rift as defined by Machette (1998). Although the historical seismicity in the region has been low (Figure 2), the site has undoubtedly been shaken by past large prehistoric earthquakes caused by active regional faults and in historical times, as recently as 1887 (Figures 2 to 4). In this study, site-specific seismic hazard analyses of Lake Roberts Dam have been performed incorporating new data on seismic sources and ground motion prediction models.

Lake Roberts Dam was constructed between 1962 and 1963. It is located on Sapillo Creek, a tributary to the Gila River, approximately 29 km north of Silver City. Specifically, the dam is located in Section 2, Township 15 South, and Range 13 West of the New Mexico Principal Meridian. The existing dam is a zoned earthfill embankment dam with a maximum height of about 17 m from streambed to dam crest. The dam crest length is approximately 92 m from the right (north) abutment to the spillway and the crest width is approximately 5.5 m. The spillway is 24 m wide and is located at the left (south) abutment. The dam crest is at elevation 1845 m (original datum). The dam impounds about 870 acre-feet with a surface area of 70 acres at the spillway crest elevation of 1839 m (original datum).

The objectives of these analyses are to estimate the levels of ground motions that could be exceeded at specified annual frequencies (or return periods) at the damsite based on a probabilistic seismic hazard analysis (PSHA). We have computed the hazard at the damsite at the top of unweathered rock beneath alluvium and weathered rock in the foundation. A deterministic seismic hazard analysis (DSHA) was also performed to compare against the PSHA results.

In this evaluation, the available geological and seismological data, including information collected as part of this study, were used to evaluate and characterize potential seismic sources, the likelihood of earthquakes of various magnitudes occurring on or within those sources, and the likelihood of the earthquakes producing ground motions over a specified level. The PSHA methodology used in this study allows for the explicit inclusion of the range of possible interpretations in components of the seismic hazard model, including seismic source characterization and ground motion estimation. Uncertainties in models and parameters are incorporated into the PSHA through the use of logic trees.

This report describes the PSHA methodology, the seismotectonic setting and the historical seismicity of the site region, the inputs including the seismic source characterization, the ground motion prediction models, and both the PSHA and DSHA hazard calculations. The report concludes with a discussion of the estimated ground motions for the dam and comparisons with the U.S. Geological Survey (USGS) National Seismic Hazard Maps.

1.1 SCOPE OF WORK

The following describes the specific tasks performed in this study.

Task 1. Seismic Source Characterization

We identified and characterized the seismic source parameters for all local and regional faults that may be significant to the site in terms of ground shaking hazard. These fault parameters included geometry and rupture dimensions, maximum earthquake, nature and amount of slip for

the maximum earthquake, and rate and nature of earthquake recurrence. The background seismicity was also characterized for the hazard analysis.

Task 2. Evaluation of the Historical Seismicity

The historical seismicity was evaluated in the vicinity of the site based on a historical catalog compiled for the site region. Historical ground shaking was evaluated at the site from past events, e.g., 1887 moment magnitude (**M**) 7.4 Sonora, Mexico earthquake.

Task 3. Site Characterization

All readily available geologic, geotechnical, and geophysical data were reviewed and evaluated to characterize the geologic conditions at the site. Of particular importance are information on shear-wave velocity (V_s), which is an input into the recently developed Pacific Earthquake Engineering Research (PEER) Center's Next Generation of Attenuation (NGA) ground motion prediction models.

Task 4. PSHA

We performed a PSHA to evaluate the probabilities of exceeding certain ground motion levels at the site based on the available information and data on seismic sources (Task 1), historical seismicity (Task 2), and site conditions (Task 3) using the NGA ground motion models. We also calculated deterministic spectra for the controlling maximum earthquake to compare with the PSHA results.

Task 5. Safety Evaluation Earthquake Ground Motions

We developed site-specific acceleration response spectra for the horizontal component. The spectra were calculated for 5% damping.

Task 6. Final Report

The approach and results of all tasks are described in this report. This draft report was reviewed internally, transmitted to the client for review, and the resulting comments will be addressed and incorporated into the final report.

1.2 ACKNOWLEDGMENTS

This study was supported by U.S. Fish and Wildlife Service. Our thanks to URS Project Manager Gregg Batchelder-Adams for his support. Thanks to Melinda Lee, Fabia Terra, and Jason Boomer for their assistance in preparing this report.

The PSHA approach used in this study is based on the model developed principally by Cornell (1968). The occurrence of earthquakes on a fault is assumed to be a Poisson process. The Poisson model is widely used and is a reasonable assumption in regions where data are sufficient to provide only an estimate of average recurrence rate (Cornell, 1968). When there are sufficient data to permit a real-time estimate of the occurrence of earthquakes, the probability of exceeding a given value can be modeled as an equivalent Poisson process in which a variable average recurrence rate is assumed. The occurrence of ground motions at the site in excess of a specified level is also a Poisson process, if (1) the occurrence of earthquakes is a Poisson process, and (2) the probability that any one event will result in ground motions at the site in excess of a specified level is independent of the occurrence of other events.

The probability that a ground motion parameter "Z" exceeds a specified value "z" in a time period "t" is given by:

$$p(Z > z) = 1 - e^{-v(z) \cdot t} \tag{1}$$

where $v(z)$ is the annual mean number (or rate) of events in which Z exceeds z . It should be noted that the assumption of a Poisson process for the number of events is not critical. This is because the mean number of events in time t , $v(z) \cdot t$, can be shown to be a close upper bound on the probability $p(Z > z)$ for small probabilities (less than 0.10) that generally are of interest for engineering applications. The annual mean number of events is obtained by summing the contributions from all sources, that is:

$$v(z) = \sum_n v_n(z) \tag{2}$$

where $v_n(z)$ is the annual mean number (or rate) of events on source n for which Z exceeds z at the site. The parameter $v_n(z)$ is given by the expression:

$$v_n(z) = \sum_i \sum_j \beta_n(m_i) \cdot p(R=r_j|m_i) \cdot p(Z>z|m_i,r_j) \tag{3}$$

where:

- $\beta_n(m_i)$ = annual mean rate of recurrence of earthquakes of magnitude increment m_i on source n ;
- $p(R=r_j|m_i)$ = probability that given the occurrence of an earthquake of magnitude m_i on source n at distance R , r_j is the closest distance increment from the rupture surface to the site;
- $p(Z > z|m_i,r_j)$ = probability that given an earthquake of magnitude m_i at a distance of r_j , the ground motion exceeds the specified level z .

The calculations were made using the computer program HAZ38 developed by N. Abrahamson. This program has been validated in the Pacific Earthquake Engineering Research (PEER) Center-sponsored "Validation of PSHA Computer Programs" Project (Thomas *et al.*, 2010).

2.1 SEISMIC SOURCE CHARACTERIZATION

Two types of earthquake sources are characterized in this PSHA: (1) fault sources; and (2) areal source zones (Section 4.1). Fault sources are modeled as three-dimensional fault surfaces and details of their behavior are incorporated into the source characterization. Areal source zones are regions where earthquakes are assumed to occur randomly. Seismic sources are modeled in the hazard analysis in terms of geometry and earthquake recurrence.

The geometric source parameters for faults include fault location, segmentation model, dip, and thickness of the seismogenic zone. The recurrence parameters include recurrence model, recurrence rate (slip rate or average recurrence interval for the maximum event), slope of the recurrence curve (*b*-value), and maximum magnitude. Clearly, the geometry and recurrence are not totally independent. For example, if a fault is modeled with several small segments instead of large segments, the maximum magnitude is lower, and a given slip rate requires many more small earthquakes to accommodate a cumulative seismic moment. For areal source zones, only the areas, maximum magnitude, and recurrence parameters (based on the historical earthquake record) need to be defined.

Uncertainties in the seismic source parameters as described below, which were sometimes large, were incorporated into the PSHA using a logic tree approach (Figure 5). In this procedure, values of the source parameters are represented by the branches of logic trees with weights that define the distribution of values. A sample logic tree for a fault is shown on Figure 5. In general, three values for each parameter were weighted and used in the analysis. Statistical analyses by Keefer and Bodily (1983) indicate that a three-point distribution of 5th, 50th, and 95th percentiles weighted 0.185, 0.63, and 0.185 (rounded to 0.2, 0.6, and 0.2), respectively, is the best discrete approximation of a continuous distribution. Alternatively, they found that the 10th, 50th, and 90th percentiles weighted 0.3, 0.4, and 0.3, respectively, can be used when limited available data make it difficult to determine the extreme tails (i.e., the 5th and 95th percentiles) of a distribution. Note that the weights associated with the percentiles are not equivalent to probabilities for these values, but rather are weights assigned to define the distribution. We generally applied these guidelines in developing distributions for seismic source parameters with continuous distributions (e.g., M_{\max} , fault dip, slip rate or recurrence) unless the available data suggested otherwise. Estimating the 5th, 95th, or even 50th percentiles is typically challenging and involves subjective judgment given limited available data.

Source Geometry

In the PSHA, it is assumed that earthquakes of a certain magnitude may occur randomly along the length of a given fault or segment. The distance from an earthquake to the site is dependent on the source geometry, the size and shape of the rupture on the fault plane, and the likelihood of the earthquake occurring at different points along the fault length. The distance to the fault is defined to be consistent with the specific ground motion prediction model used to calculate the ground motions. The distance, therefore, is dependent on both the dip and depth of the fault plane, and a separate distance function is calculated for each geometry and each ground motion model. The size and shape of the rupture on the fault plane are dependent on the magnitude of the earthquake; larger events rupture longer and wider portions of the fault plane. We modeled the rupture dimensions following the magnitude-rupture length relationship of Wells and Coppersmith (1994).

Fault Recurrence

The recurrence relationships for the faults are modeled using the truncated-exponential (Gutenberg-Richter) characteristic earthquake, and the maximum magnitude recurrence models (Section 4.1.1). These models are weighted (Figure 5) to represent our judgment on their applicability to the sources. For the areal source zones, only a truncated exponential recurrence model is assumed to be appropriate.

We have used the general approach of Molnar (1979) and Anderson (1979) to arrive at the recurrence for the truncated exponential model. The number of events exceeding a given magnitude, $N(m)$, for the truncated exponential relationship is

$$N(m) = \alpha(m^o) \frac{10^{-b(m-m^o)} - 10^{-b(m^u-m^o)}}{1 - 10^{-b(m^u-m^o)}} \quad (4)$$

where $\alpha(m^o)$ is the annual frequency of occurrence of earthquakes greater than the minimum magnitude, m^o ; b is the Gutenberg-Richter parameter defining the slope of the recurrence curve; and m^u is the upper-bound magnitude event that can occur on the source. A m^o of **M** 5.0 was used for the hazard calculations because smaller events are not considered likely to produce ground motions with sufficient energy to damage well-designed structures.

We have included the model that the faults rupture with a "characteristic" magnitude on specific segments; this model is described by Aki (1983) and Schwartz and Coppersmith (1984). For the characteristic model, we have used the numerical model of Youngs and Coppersmith (1985). In the characteristic model, the number of events exceeding a given magnitude is the sum of the characteristic events and the non-characteristic events. The characteristic events are distributed uniformly over a ± 0.3 magnitude unit around the characteristic magnitude, and the remainder of the moment rate is distributed exponentially using the above equation with a maximum magnitude one unit lower than the characteristic magnitude (Youngs and Coppersmith, 1985).

The maximum magnitude model can be regarded as an extreme version of the characteristic model. We adopted the model proposed by Wesnousky (1986). In the maximum magnitude model, there is no exponential portion of the recurrence curve, i.e., no events can occur between the minimum magnitude of **M** 5.0 and the distribution about the maximum magnitude.

The recurrence rates for the fault sources are defined by either the slip rate or the average return time for the maximum or characteristic event and the recurrence b -value. The slip rate is used to calculate the moment rate on the fault using the following equation defining the seismic moment:

$$M_o = \mu A D \quad (5)$$

where M_o is the seismic moment, μ is the shear modulus, A is the area of the rupture plane, and D is the slip on the plane. Dividing both sides of the equation by time results in the moment rate as a function of slip rate:

$$\dot{M}_o = \mu A S \quad (6)$$

where \dot{M}_o is the moment rate and S is the slip rate. M_o has been related to moment magnitude, M , by Hanks and Kanamori (1979):

$$M = 2/3 \log M_o - 10.7 \quad (7)$$

Using this relationship and the relative frequency of different magnitude events from the recurrence model, the slip rate can be used to estimate the absolute frequency of different magnitude events.

The average return time for the characteristic or maximum magnitude event defines the high magnitude (low likelihood) end of the recurrence curve. When combined with the relative frequency of different magnitude events from the recurrence model, the recurrence curve is established.

2.2 GROUND MOTION PREDICTION MODELS

To characterize the ground motions at a specified site as a result of the seismic sources considered in the PSHA and DSHA, we used empirical ground motion prediction equations (models) for PGA and spectral accelerations. The models used in this study were selected on the basis of the appropriateness of the site conditions and tectonic environment for which they were developed (Figure 5; Section 4.2).

The uncertainty in ground motion prediction models was included in the PSHA by using the log-normal distribution about the median values as defined by the standard error associated with each model. Three standard deviations about the median value were included in the analysis.

The following describes the seismotectonic setting and historical seismicity of the site region as defined in Figure 2. An understanding of the seismotectonic setting and historical seismicity of a site provides the framework in which the earthquake potential of geologic structures in a region can be characterized.

3.1 SEISMOTECTONIC SETTING

Lake Roberts Dam is located at the juncture of several tectonic provinces: (1) Mogollon-Datil volcanic field and the Rio Grande rift (RGR) to the north and east, respectively; (2) the southern Basin and Range Province to the west, and the Transition Zone between the Colorado Plateau and Basin and Range; and (3) the largely undeformed Colorado Plateau to the north (Figure 1).

The Southern Basin and Range Province is characterized by a block-faulted topography of alternating mountain range blocks bounded by moderate-to steeply-dipping normal faults and intervening valleys. The mountains are comprised of igneous, metamorphic and indurated sedimentary rocks of Precambrian through to Tertiary age, while the valleys are filled with a relatively undeformed sequence of fluvial and lacustrine sediments of Oligocene to Pleistocene age. The present-day structural basins resulted from a period of extensive normal faulting, the Basin and Range disturbance, that began 10 to 13 Ma. Landforms indicating tectonic inactivity dominate the region today, implying cessation of major extension at some time in the late Miocene or Pliocene (Menges and McFadden, 1981). This is reflected by the low levels of historical seismicity and sparse evidence for Quaternary faulting in southern Arizona and southwestern New Mexico. The Southern Basin and Range Province is dominated by northwest-southeast-striking normal faults; however, the study area encompasses the transition from this northwest-southeast structural grain to a more north-south orientation as the province extends into northern Mexico.

Note that Machette (1998) places the western boundary of the southern Rio Grande rift in the southwestern part of New Mexico further west to encompass the extent of north-trending Quaternary normal faults as far west as the Arizona/New Mexico border. According to this assessment, the Lake Roberts Dam is located in the Rio Grande rift (Figure 1). Dorsey (1998) notes that the only similarity between the Transition Zone and the southern Rio Grande rift is the dominantly northwest trend of the faults.

3.2 HISTORICAL SEISMICITY

The Lake Roberts Dam is located in a region characterized by a low-level of historical seismicity although seismographic coverage of the region has been poor. A notable earthquake of **M** 7.4 occurred on 5 May 1887 in northern Sonora, Mexico (DuBois *et al.*, 1982; Suter and Contreras, 2002; Figure 4). This earthquake ruptured the Pitaycachi fault about 200 km southwest of the site and was felt as far away as Albuquerque, New Mexico, and El Paso, Texas. Intensities of Modified Mercalli (MM) VII to VIII are estimated for the site (Figure 4).

The largest earthquake to occur in the site region was an earthquake on 5 July 1934 about 38 km south of the damsite (Figure 2). The magnitude of the event, Richter local magnitude (M_L) 4.3, is based on its maximum intensity of MM V.

Also a M_L 4.0 earthquake was located 43 km northwest of the damsite on 1 July 1939 (Figure 2). The location uncertainties of both this event and the 1934 event are large, probably on the order of tens of kilometers.

In this study, all known seismic sources which could potentially generate strong ground shaking at the site were characterized. Seismic source characterization is concerned with three fundamental elements: (1) the identification of significant sources of earthquakes; (2) the maximum size of these earthquakes; and (3) the rate at which they occur. Ground motion prediction models, the other essential input into the hazard analysis, are also described.

4.1 EARTHQUAKE SOURCES

The earthquake sources, active faults, and background seismicity are described in the following.

4.1.1 Quaternary Faults

Faults were included in the analyses that were judged to potentially contribute to the probabilistic hazard at the site because of their activity, length, or proximity to the site region. We included known faults within 100 km of the sites showing evidence for late Quaternary activity (< 130 ka) or repeated Quaternary (< 1.6 Ma) activity (Figure 3). We also considered longer, more active faults in southern California, such as the southern San Andreas fault, because from previous analyses in the region (e.g., Wong *et al.*, 2011), we know these major fault sources can be significant contributors to the hazard at longer periods, despite their great distances.

URS recently characterized the active faulting in the region surrounding the Chino (Wong *et al.*, 2006) and the Morenci (Wong *et al.*, 2011) mines. For this analysis, we updated and revised the input from these previous analyses. We reviewed fault information from the U.S. Geological Survey (USGS) Quaternary Fault and Fold Database website (URL: <http://qfaults.cr.usgs.gov>), and added faults as necessary. We included 27 “local” fault sources and four fault sources located in Southern California for this analysis. Note that we did not include a nearby unnamed west-northwest-striking normal fault, which was discussed in the site investigation report (URS, 2011) and mapped by Ratte and Gaskill (1975). We did not include this fault in our analysis because it is so short (about 4.2 km long) and it was not included in the Quaternary fault compilation of Machette *et al.* (1998) or the USGS Quaternary Fault and Fold Database, probably because it does not show strong enough evidence for Quaternary activity. However, this fault has not been studied in detail and little is known about its behavior. Ratte and Gaskill (1975) dash this fault entirely within the Gila Conglomerate. It apparently offsets sediments of the Gila Conglomerate down against a Tertiary basalt by at least ~15 m (50 feet) (URS, 2011). The age of this offset is unknown, but the Gila conglomerate is primarily Pliocene and early Pleistocene alluvium and basin fill. Thus, even if the fault has had Quaternary activity, it appears to have a low rate of activity (likely < 0.009 mm/yr), and it would not contribute significantly to the hazard.

Figure 3 shows the location of the local fault sources included in the analysis. These faults all lie within the Colorado Plateau – Basin and Range transition zone or the southern Rio Grande rift, and all the faults in this region have low to moderate rates of activity (slip rates that are generally < 0.5 mm/yr). Table 1 summarizes the parameters used in our analysis for these local faults. A general discussion of the local fault source parameters is also included below. Faults are listed alphabetically, and nomenclature and numbers shown in Table 1 generally follow those used by the USGS database.

The southern California fault sources included in our analysis were: the southern San Andreas, Elsinore, San Jacinto and Imperial faults. These are all major strike-slip fault zones that accommodate dextral motion between the Pacific and North American Plates. They have much higher rates of activity than the local fault sources (slip rates that are generally >1 mm/yr). The southern California faults are also generally capable of larger magnitude earthquakes (as large as **M** 8 in some cases) than the local faults. The southern California faults have been extensively studied and their rupture behavior is complex, necessitating a complex seismic source model to address variability and uncertainties. Tables 2a through 2d summarize parameters used in our analysis for the southern California fault sources. These parameters are largely after the 2007 California Geological Survey/U.S. Geological Survey Uniform California Earthquake Rupture Forecast (UCERF) model (WGCEP, 2008), and are discussed in more detail in Wong *et al.* (2009). Because of its particular importance at long periods, we also include a very brief discussion of the southern San Andreas fault zone below.

Fault parameters required in the probabilistic hazard analysis include: (1) rupture model (including independent single plane and potentially linked models); (2) probability of activity; (3) fault geometry including rupture length, rupture width, fault orientation, and sense of slip; (4) maximum magnitude [M_{\max}]; and (5) earthquake recurrence including both recurrence model and rates. These parameters are generally discussed further below. Selected faults that contribute the most to the hazard are specifically discussed in subsequent sections.

Maximum magnitudes were estimated using the empirical relationships of Wells and Coppersmith (1994) for all types of faults, as noted in the footnotes of Table 1. Recurrence models can significantly impact hazard calculations and we considered truncated exponential, maximum magnitude, and characteristic recurrence models for this analysis. Observations of historical seismicity and paleoseismic investigations suggest that characteristic behavior is more likely for individual faults, whereas seismicity in areal zones best fits a truncated exponential model (Schwartz and Coppersmith, 1984; Youngs and Coppersmith, 1985). The maximum magnitude model is an extreme version of the characteristic model (Wesnousky, 1986). We favored (weighted 0.6) the characteristic model for all fault sources and assigned equal weights of 0.2 to the exponential and maximum magnitude models (Figure 5).

In assigning probabilities of activity for each fault source, we considered both the likelihood that the fault is structurally capable of independently generating earthquakes, and the likelihood that it is still active within the modern stress field. We incorporated many factors in assessing these likelihoods, such as: orientation in the modern stress field, fault geometry (length, continuity, and dip), relation to other faults, age of youngest movement, rates of activity, geomorphic expression, amount of cumulative offset, and any evidence for a non-tectonic origin. Faults with definitive evidence for repeated Quaternary activity were generally assigned probabilities of being active (seismogenic) of 1.0 (Table 1). The probability of activity for faults that do not show definitive evidence for repeated Quaternary activity was individually judged based on available data and the criteria explained above. Resulting values range from 0.7 to 1.0 (Table 1) and the specific reasons for assigning probabilities less than 1.0 to a particular fault are generally given in the comments column of Table 1.

As recurrence interval data are generally lacking for local faults, we used slip rates to characterize rates of fault activity (Table 1). We considered all available long- (≤ 1.6 Ma) and

short-term (≤ 130 ka) data in developing slip rate distributions, but we preferred short-term data whenever possible. In addition to the time period, we also considered the type and quality of data in determining rates. Preferred slip rates (generally weighted 0.6) are primarily based on data in Machette *et al.* (1998) as noted in the comments column of Table 1. Maximum and minimum values (each generally weighted 0.2) are typically selected to represent 95th and 5th percentile values after the approach of Wong *et al.* (2004) unless the available data suggest otherwise as noted in the comments column of Table 1.

The most significant faults, the Mockingbird Hill, Mogollon and southern San Andreas faults are discussed further below.

Mockingbird Hill Fault Zone and Mogollon Fault

The Mockingbird Hill fault zone (#2013) and the Mogollon fault (#2012) are about 32 and 31 km west of Lake Roberts Dam (Figure 3). They are generally north-northwest striking, west-southwest-dipping, normal-slip, Quaternary faults that lie directly along strike of each other and bound the eastern margin of the Mogollon and Mangas graben. Based on this, and the individual short length of the Mockingbird Hill fault zone (< 7 km), we considered these faults to be linked together, rupturing coseismically with a maximum rupture length of 22 km (Figure 3; Table 1). This length yields a preferred maximum magnitude of **M** 6.6 for this source in our PSHA (Table 1). For the DSHA, we included a scenario of **M** 6.9 (the same as our upper bound maximum magnitude in the PSHA) for rupture of the Mockingbird Hill and Mogollon faults because these faults have not been studied in detail and their paleoseismic behavior is not well understood. This allows for the possibility that the surface rupture length may be underestimated for these somewhat short, poorly known faults.

Little is known about the Quaternary rates of activity for either the Mockingbird Hill or Mogollon faults. The Mockingbird Hill fault zone offsets mid-Pleistocene Wild Horse Mesa pediment-terrace deposits (Leopoldt, 1981), however, amounts of offset are unknown. The Mogollon Hill fault offsets erosional remnants of the Plio-Pleistocene Clum-Mine Ridge pediment-terrace gravel about 110 m (Leopoldt, 1981). Assuming this is vertical slip that occurred on a $\sim 60^\circ$ dipping fault since 1.6 Ma yields an estimated preferred dip-slip rate of 0.08 mm/yr (Table 1). Given the lack of information on this fault, we used the approach of Wong *et al.* (2004) to define a slip rate distribution and account for uncertainties in rates of activity on these faults.

Southern San Andreas Fault Zone

The San Andreas fault accommodates the majority of the motion between the Pacific and North American plates. The fault shows scarps on Holocene alluvium, right-laterally offset drainages, closed depressions, and shutter ridges. At least one earthquake, a **M** 7.9 event in 1857, ruptured the southern half of the fault during historical time. Extensive paleoseismic investigations have revealed a history of surface faulting events along the fault during Holocene time (WGCEP, 2008). Based on differing paleoseismic chronologies, slip rates, slip-per-event, changes in fault geometry, and geomorphic expression, the San Andreas fault has been divided into a number of rupture segments (WGCEP, 2008). In southern California, these segments include, from north to south, the Parkfield, Cholame, Carrizo, Big Bend, Mojave North and South, San Bernardino North and South, San Gorgonia Pass-Garnet Hill, and Coachella Valley. Although each segment

has a distinct paleoseismic history, neighboring segments appear to have ruptured simultaneously in a number of paleoevents. The 1857 earthquake ruptured the Cholame, Carrizo, Mojave, and part of the San Bernardino Mountains segments.

Geologic mapping and seismicity studies indicate that the San Andreas fault is a vertical structure, thus we model the fault dip as $90^\circ \pm 10^\circ$. We adopt the fault segmentation of WGCEP (2008) and the slip rates and maximum earthquakes assigned in their Southern California earthquake model (Wong *et al.*, 2009). The slip rates for individual segments are based on detailed paleoseismic investigations. In addition to rupture of individual segments, we also consider multi-segment rupture, similar to the ‘cascade’ model of WGCEP (2008), which allows for rupture on contiguous segments. Our multi-segment model allows for an **M** 8 event anywhere on the southern San Andreas fault between Cholame and the southern end of the Salton Trough (Wong *et al.*, 2009). The best estimate slip rate is 30 mm/yr, with the range of uncertainty reflecting the maxima and minima calculated from paleoseismic studies on all the fault segments considered.

4.1.2 Background Seismicity

In state-of-the-practice seismic hazard evaluations, the hazard from background (random) earthquakes is addressed. Background earthquakes are those events that do not appear to be associated with known geologic structures. They occur on crustal faults that exhibit no surficial expression (buried faults) or are unmapped due to inadequate studies. In this analysis, we address the hazard from background earthquakes through the use of a regional source zone for western New Mexico, and use Gaussian smoothing.

In the western U.S., the conventional approach has been to assume that the minimum threshold for surface faulting represents the upper size limit for background earthquakes. In much of the western U.S., this threshold ranges from **M** 6 to $6\frac{1}{2}$ (e.g., dePolo, 1994). It is believed that larger earthquakes will be accompanied by surface rupture, and repeated events of this size will produce recognizable fault-related geomorphic features. In this study, we have adopted a maximum magnitude of **M** $6\frac{1}{2} \pm \frac{1}{4}$.

Earthquake recurrence estimates are required for each seismic source zone to calculate the hazard. The recurrence relationship assumes the truncated exponential form of the Gutenberg-Richter relationship of the $\log N = a - bM$. Although the site is located within the Rio Grande rift as defined by Machette (1998) (Figure 1), the historical seismicity in southwestern New Mexico is too sparse to calculate recurrence parameters. Thus we assume that the earthquake recurrence is relatively uniform throughout all of western New Mexico. The recurrence curve was computed for western New Mexico, including the Colorado Plateau, the Transition Zone, and the Rio Grande rift. The computed *b*-value is 0.65 and the *a*-value -3.65. Based on this recurrence, **M** 5.0 and **M** 6.0 earthquakes occur approximately every 52 and 247 years, respectively, in western New Mexico. The uncertainties in these values are very large, possibly on the order of several decades or more.

Because of the limited duration and incompleteness of the historical catalog and the small number of events and their narrow magnitude range used in the recurrence calculations, uncertainties in the recurrence parameters for the background seismicity are large. To incorporate the uncertainties into the PSHA, we used three *b*-values for the regional seismic

source zone, the best estimate, and plus and minus 0.1 values, weighted 0.6, 0.2, and 0.2, respectively. An inspection of the resulting recurrence intervals for **M** 5 and 6 events was performed to check the reasonableness of the three *b*-values. The *a*-values were held fixed because the recurrence curve was better constrained at the smaller magnitudes.

In addition to the traditional approach of using areal source zones (assuming uniformly distributed seismicity), we also used Gaussian smoothing (Frankel, 1995), as was done for the USGS National Hazard Maps, to address the hazard from background earthquakes in the PSHA. In this approach, instead of assuming that the background seismicity is uniformly (randomly) distributed throughout a volume of the crust, as is the case in the use of seismic source zones, spatial stationarity in the distribution of the historical seismicity is retained by smoothing. We smoothed the historical background seismicity using a spatial window of 15 km. The two approaches, areal source zones and Gaussian smoothing, were weighted equally in calculating the background seismicity hazard for the maps.

4.2 GROUND MOTION PREDICTION MODELS

Several factors control the level and character of earthquake ground shaking. These main factors are: (1) rupture dimensions, geometry, and orientation of the causative fault; (2) distance from the causative fault; (3) magnitude of the earthquake; (4) the rate of attenuation of the seismic waves along the propagation path from the source to the site; and (5) site factors including the effects of near-surface geology, particularly from soils and unconsolidated sediments. Other factors, which vary in their significance depending on specific conditions, include slip distribution along the fault, rupture process (e.g., directivity), footwall/hanging-wall effects, and the effects of crustal structure such as basin effects.

Several parameters may be used to characterize earthquake ground motions. The common parameters include: peak ground acceleration, velocity, and displacement; response spectral accelerations or velocities; duration; and time histories of acceleration, velocity, or displacement. In this analysis, we have estimated only peak horizontal accelerations.

The traditional approach in estimating ground motions in seismic hazard analysis utilizes empirical ground motion prediction equations (models) that are derived from strong motion data. Attenuation is defined as the decrease in amplitude or intensity of seismic waves with distance. Ground motion prediction models depict the decrease in amplitude of a specified ground motion parameter with distance as a function of magnitude (Abrahamson and Shedlock, 1997). This decrease due to attenuation results from a number of factors including geometrical spreading, damping or absorption by the earth, scattering, reflection, refraction, diffraction, and wave conversion. Empirical models have been developed in regions where there are numerous strong ground motion recordings by applying statistical regression methods to these data. Because the data correspond to geologic conditions and earthquakes typical of the region, they are generally applicable only in that region. However, they may also be used in another area with similar seismotectonic characteristics.

No empirical strong motion records exist for moderate to large earthquakes occurring in New Mexico or the Southwest. In this analysis, we used the NGA relationships of Abrahamson and Silva (2008), Campbell and Bozorgnia (2008), Chiou and Youngs (2008), and Boore and Atkinson (2008). These relationships were the result of the NGA Project and have been

extensively reviewed by the USGS and others. These models have been used in the 2008 National Hazard Maps (Section 5.2).

All models are appropriate for extensional normal faulting although admittedly they are not well constrained due to a general paucity of strong motion data for normal faulting earthquakes, particularly at $M \geq 6$. The models were weighted equally to estimate the ground motions at the damsite.

There are no site-specific V_S data for the foundation conditions beneath Lake Roberts Dam that would provide an estimate of V_{S30} (average shear-wave velocity in the top 30 m), which is a required input in the NGA relationships. The V_{S30} accounts for site response effects in the NGA-modeled ground motions.

The dam foundation consists of layers of basalt and volcanic breccias overlain by a thick (on the order of 12 m) alluvial deposit based on exploration boreholes (Boyle Engineering, 2007). The alluvial deposit encountered in the dam foundation consists primarily of sand and gravel with a small percentage of fines. Bedrock encountered under the dam consists of alternating layers of basalt and breccia and includes a thin sandstone layer interbedded within the volcanic deposits.

Seismic refraction surveys were conducted as part of the geotechnical evaluation for Lake Roberts Dam (URS, 2011). Six seismic refraction lines were completed during the field program. Results of the seismic refraction data suggest the presence of a three-layer model of the subsurface for most of the lines conducted. Based on this model, the dam is underlain by about 12 m of alluvium and up to 16 m of weathered basalt. Assuming a Poisson's ratio of 0.30 (Payne, 2007), V_S in the unweathered rock ranges from 850 to 1,260 m/sec with large uncertainties. Thus, we adopted a mean V_{S30} of 1,000 m/sec for the damsite with a large epistemic uncertainty of ± 200 m/sec to address the uncertainty in the V_{S30} value and the natural variability beneath the damsite.

Other input parameters include $Z_{1.0}$, the depth of a V_S of 1.0 km/sec and $Z_{2.5}$, the depth to a V_S of 2.5 km/sec. Both parameters were used by some of the developers as proxies for basin effects. $Z_{1.0}$ is used by Chiou and Youngs (2008) and Abrahamson and Silva (2008) and $Z_{2.5}$ is only used in one model, Campbell and Bozorgnia (2008). Due to the lack of site-specific data, the default values of $Z_{1.0}$ and $Z_{2.5}$, based on the V_{S30} from equations provided by the developers, were used in the PSHA. Other parameters such as depth to the top of rupture (zero for all surficial faults unless specified otherwise), dip angle, rupture width, and aspect ratio of each fault are specified or calculated within the PSHA code.

The PSHA results for Lake Roberts Dam are described below and they are compared with the USGS National Hazard Maps and deterministic ground motions.

5.1 HAZARD RESULTS

The results of the PSHA are presented in terms of ground motion as a function of annual exceedance probability. This probability is the reciprocal of the average return period. Figure 6 shows the mean, median (50th percentile), 5th, 15th, 85th, and 95th percentile hazard curves for PGA for the damsite for a V_{S30} of 800 m/sec. The hazard results using the other two V_{S30} values are similar. The fractiles indicate the range of uncertainties about the mean hazard. At a return period of 2,500 years, there is a factor of 3 difference between the 5th and 95th percentile hazard at the dam (Figure 6). The 1.0 sec horizontal SA hazard curve is shown on Figure 7. The PGA and horizontal spectral accelerations (SA) for the return periods of 2,475, 5,000, and 10,000 years are listed on Table 3.

The contributions of the various seismic sources to the mean PGA hazard are shown on Figure 8. Background seismicity as addressed through the regional source zone and gridded seismicity controls the hazard at all return periods. The Mockingbird Hill/Mogollon fault also contributes to the PGA hazard (Figure 8). At long-period ground motions such as 1.0 sec SA, the Southern San Andreas fault and background seismicity control the hazard (Figure 9).

By deaggregating the PGA and 1.0 sec horizontal SA hazard by magnitude (M) and distance (D) bins, the contributions by events at a return periods of 2,475 and 10,000 years can be evaluated (Figures 10 to 13). At PGA, most of the hazard at the damsite is from earthquakes of M 5 to 6.75 at distances less than 40 km, corresponding to the background seismicity (Figures 10 and 11). At longer spectral periods, e.g., 1.0 sec SA, the background earthquakes contribute to the hazards but with a significant peak at larger magnitudes from the Southern San Andreas fault (Figures 12 and 13).

Based on the magnitude and distance bins (Figures 10 to 13), the controlling earthquakes as defined by the modal magnitude M and modal distance D can be calculated (Table 4). The controlling event is a moderate-size background earthquake of about M 6.5 at 30 to 35 km.

Figures 14 and 15 illustrate the sensitivity of the mean PGA and 1.0 sec horizontal SA hazard to the choice of ground motion prediction models. Each hazard curve is labeled with one of the four NGA models calculated using only that model. At both PGA and 1.0 sec SA, the Campbell and Bozorgnia (2008) model gives higher hazard than the other models (Figures 14 and 15).

5%-damped horizontal UHS for the return periods of 2,475 and 10,000 years are shown on Figure 16 for all three V_{S30} values. The lower V_{S30} of 800 m/sec has a spectrum that envelopes the other two UHS. To address the epistemic uncertainty in the inferred V_{S30} and the variability in V_{S30} across the site, our recommended horizontal spectra for design analyses are the enveloped UHS (Figure 17).

5.2 COMPARISON WITH THE USGS NATIONAL HAZARD MAPS

In the 2008 versions of the USGS's National Hazard Maps, which are the basis for the current U.S. building code, Petersen *et al.* (2008) estimated probabilistic ground motions for the U.S. for the exceedance probability of 2% in 50 years (2,475-year return period) and a firm rock site

condition (NEHRP site class B/C), which is characterized by a V_{S30} of 760 m/sec. The USGS 2,475-year return period rock PGA at the damsite is 0.11 g (Petersen *et al.*, 2008) compared to our 2,475-year return period value of 0.09 g for a V_{S30} of 800 m/sec. Despite the differences in approaches, the values compare favorably.

5.3 COMPARISON WITH DETERMINISTIC HAZARD ANALYSIS

To compare the UHS with a traditional deterministic spectrum, the same ground motion prediction models used in the PSHA were used to calculate 84th percentile 5%-damped acceleration response spectra for the closest known active fault, the Mockingbird Hill/Mogollon fault (Figure 18; Table 5). The source-to-site (rupture) distance is 31 km and the maximum magnitude, a value between the best estimate value and the two-sigma value in Table 1, is **M** 6.9. The three values of V_{S30} were run and the envelope of the three spectra are shown on Figure 18. The lognormal mean 84th percentile spectrum is compared against the spectra in Figure 19. The 84th percentile spectrum lies between the 5,000 and 10,000-year return period UHS up to a spectral period of about 0.4 sec and coincides with the 10,000-year return period UHS at longer periods. This observation is typical of sites in the southern Basin and Range Province located near active faults that have low slip rates (Wong, 2009).

- Abrahamson, N., and Shedlock, K., 1997, Some comparison between recent ground-motion relations: *Seismological Research Letters*, v. 68, p. 9-23.
- Abrahamson, N.A. and Silva, W.J., 2008, Summary of the Abrahamson and Silva NGA ground motion relations: *Earthquake Spectra*, v. 24, p. 67-97.
- Aki, K., 1983, Seismological evidence in support of the existence of “Characteristic Earthquakes”: *Earthquake Notes*, v. 54, p. 60-61.
- Anderson, J.G., 1979, Estimating the seismicity from geological structure for seismic risk studies: *Bulletin of the Seismological Society of America*, v. 69, p. 135-158.
- Boore, D.M., and Atkinson, G.M., 2008, Ground motion predictive equations for the average horizontal component of PGA, PGV, and 5% damped PSA at spectral periods between 0.01s to 10.0s: *Earthquake Spectra*, v. 24, p. 99-138.
- Boyle Engineering, 2007, Lake Roberts Dam safety project, draft preliminary design report: prepared for the New Mexico Department of Game and Fish, 63 p.
- Campbell, K.W. and Bozorgnia, Y., 2008, NGA ground motion model for the geometric mean horizontal component of PGA, PGV, PGD, and 5% damped linear elastic response spectra for periods ranging from 0.01 to 10s: *Earthquake Spectra*, v. 24, p. 139-171.
- Chiou, B.S.J. and Youngs, R.R., 2008, An NGA model for the average horizontal component of peak ground motion and response spectra: *Earthquake Spectra*, v. 24, p. 173-215.
- Cornell, C.A., 1968, Engineering seismic risk analysis: *Bulletin of the Seismological Society of America*, v. 58, p. 1583-1606.
- dePolo, C. M., 1994, The maximum background earthquake for the Basin and Range Province, western North America: *Bulletin of the Seismological Society of America*, v. 84, p. 466-472.
- Dorsey, J.D., 1998, Late Tertiary evolution of the Mimbres Basin near San Lorenzo, New Mexico: M.S. Thesis, New Mexico State University, 71 p.
- DuBois, S.M., Smith, A.W., Nye, N.K., and Norwak, T.A., 1982, Arizona earthquakes, 1776-1980: *Arizona Bureau of Geology and Mineral Technology Bulletin*, v. 193, 456 p.
- Elston, W.E., 1957, Geology and mineral resources of Dwyer quadrangle, Grant, Luna, and Sierra Counties, New Mexico: *New Mexico Bureau of Mines and Mineral Resources Bulletin* 38, 86 p., 4 pls.
- Ferguson, C.A., 1988, Geology of the Tenmile Hill 7.5' quadrangle, Socorro County, New Mexico: *New Mexico Bureau of Mines and Mineral Resources Open-File Report* 283, 21 p., 2 pls.
- Ferguson, C.A., Enders, M.S., Peters, L., and McIntosh, W.C., 2000. Mid-Tertiary geology and geochronology of the Clifton-Morenci area, Greenlee and Graham Counties, Arizona: *Arizona Geological Survey, Open-file Report* 00-07, 69 p.
- Foley, L.L., LaForge, R.C., and Piety, L.A., 1988, Seismotectonic study for Elephant and Caballo Dams, Rio Grande Project, New Mexico: *U. S. Bureau of Reclamation Seismotectonic Report* 88-9, 60 p., 1 pl., scale 1:24,000.

- Frankel, A., 1995, Mapping seismic hazard in the central and eastern United States: *Seismological Research Letters*, v. 66, p. 8-21.
- Hanks, T.C. and Kanamori, H. 1979, A moment magnitude scale: *Journal of Geophysical Research*, v. 84, p. 2348-2350.
- Houser, B.B., 1994, Geology of the Late Cenozoic Alma Basin, New Mexico and Arizona: *New Mexico Geological Society Guidebook, 45th Field Conference*, p. 121-124.
- Keefer, D.I. and Bodily, S.E., 1983, Three-point approximations for continuous random variables: *Management Science*, v. 26, p. 595-609.
- Leopoldt, W., 1981, Neogene geology of the central Mangas graben, Cliff-Gila area, Grant County, New Mexico: Albuquerque, University of New Mexico, unpublished M.S. thesis, 160 p., 1 pl., scale 1:24,000.
- Machette, M.N., 1987, Preliminary assessment of Quaternary faulting near Truth or Consequences, New Mexico: U.S. Geological Survey Open-File Report 87-652, 40 p.
- Machette, M.N., 1998, Contrasts between short- and long-term records of seismicity in the Rio Grande rift – Important implications for seismic hazard assessments in areas of slow extension, *in* W.R. Lund (ed.), *Western States Seismic Policy Council Proceedings Volume, Basin and Range Province Seismic Hazards Summit*, Utah Geological Survey Miscellaneous Publication 98-2, p. 84-95.
- Machette, M.N., Personius, S.F., Kelson, K.I., Haller, K.M., and Dart, R.L., 1998, Map and data for Quaternary faults and folds in New Mexico: U.S. Geological Survey Open-File Report 98-521, 443 p.
- Machette, M.N., Personius, S.F., Menges, C.M., and Pearthree, P.A., 1986, Map showing Quaternary and Pliocene faults in the Silver City 1° x 2° quadrangle and the Douglas 1° x 2° quadrangle, southeastern Arizona and southwestern New Mexico: U.S. Geological Survey Miscellaneous Field Studies Map MF-1465-C, 12 p. pamphlet, 1 sheet, scale 1:250,000.
- Mack, G.H., Salyards, S.L., and James, W.C., 1993, Magnetostratigraphy of the Plio-Pleistocene Camp Rice and Palomas formations in the Rio Grande rift of southern New Mexico: *American Journal of Science*, v. 293, p. 49-77.
- Mack, G.H., Seager, W.R., and Leeder, M.R., 2003, Synclinal-horst basins: examples from the southern Rio Grande rift and southern transition zone of southwestern New Mexico: *Basin Research*, v. 15, p. 365-377.
- Menges, C.M. and McFadden, L.D., 1981, Evidence for the latest-Miocene to Pliocene transition from Basin-Range tectonic to post-tectonic landscape evolution in southeastern Arizona: *Arizona Geological Society Digest*, v. 13, p. 151-160.
- Menges, C.M. and Pearthree, P.A., 1983, Map of neotectonic (latest Pliocene-Quaternary) deformation in Arizona: Arizona Bureau of Geology Mineral Technology Open-File Report 83-22, 48 p., scale 1:500,000.
- Molnar, P., 1979, Earthquake recurrence intervals and plate tectonics: *Bulletin of the Seismological Society of America*, v. 69, p. 115-133.

- Payne, S.J., 2007, Modeling of the sedimentary interbedded basalt stratigraphy for the Idaho National Laboratory probabilistic seismic hazard analysis: Idaho National Laboratory INL/EXT-05-01047, 70 p.
- Pearthree, P.A., 1998, Quaternary fault data and map for Arizona: Arizona Geological Survey Open-File Report 98-24, 122 p., 1 sheet, scale 1:750,000.
- Petersen, M.D., Frankel, A.D., Harmsen, S.C., Mueller, C.S., Haller, K.M., Wheeler, R.L., Wesson, R.L., Zeng, Y., Boyd, O.S., Perkins, D.M., Luco, N., Field, E.H., Wills, C.J., and Rukstales, K.S., 2008, Documentation for the 2008 update of the United States National Seismic Hazard Maps: U.S. Geological Survey Open-File Report 2008-1128, 61 p.
- Ratté, J.C., 1981, Geologic map of the Mogollon 7.5' quadrangle, Catron County, New Mexico: U.S. Geological Survey, Geologic Quadrangle Map GQ-1557, scale 1:24,000.
- Ratte, J.C. and Gaskill, D.L., 1975, Reconnaissance geologic map of the Gila Wilderness study area: U.S. Geological Survey Miscellaneous Geologic Investigations Map I-886, scale 1:62,500.
- Schwartz, D.P. and Coppersmith, K.J., 1984, Fault behavior and characteristic earthquakes--examples from the Wasatch and San Andreas fault zones: *Journal of Geophysical Research*, v. 89, p. 5681-5698.
- Seager, W.R., Clemons, R.E., Hawley, J.W., and Kelley, R.E., 1982, Geology of northwest part of Las Cruces 1° x 2° sheet, New Mexico: New Mexico Bureau of Mines and Mineral Resources Geologic Map 53, 3 sheets, scale 1:250,000.
- Seager, W.R. and Hawley, J.W., 1973, Geology of Rincon quadrangle, Doña Ana County, New Mexico: New Mexico Bureau of Mines and Mineral Resources Bulletin 101, 42 p., 2 pls.
- Suter, M. and Contreras, J., 2002, Active tectonics of northeastern Sonora, Mexico (southern Basin and Range Province) and the 3 May 1887 M_w 7.4 earthquake: *Bulletin of the Seismological Society of America*, v. 92, p. 581-589.
- Thomas, P.A., Wong, I.G., and Abrahamson, N., 2010, Verification of probabilistic seismic hazard analysis software programs: PEER Report 2010/xx, Pacific Earthquake Engineering Research Center, College of Engineering, University of California, Berkeley, 173 p.
- URS Corporation, 2011, Lake Roberts Dam OSE File No. D-273 Grant County, New Mexico: Site Investigation Report prepared for New Mexico Department of Game and Fish.
- Wells, D. and Coppersmith, K.J., 1994, New earthquake magnitude and fault rupture parameters, Correlations among earthquake magnitude, rupture length, and fault displacement: *Bulletin of the Seismological Society of America*, v. 84, p. 974-1002.
- Wesnousky, S.G., 1986, Earthquakes, Quaternary faults, and seismic hazard in California: *Journal of Geophysical Research*, v. 91, p. 12,587-12,631.
- Wong, I.G., 2009, Comparing deterministic and probabilistic ground motions for dams in seismically active regions, western U.S.: presentation to the 2009 Western Regional Dam Safety Forum.

- Wong, I.G., Bott, J.D.J., and Olig, S.S., 1999, Probabilistic seismic hazard analysis for Caballo Dam, Rio Grande Project, South-Central New Mexico: unpublished report prepared for the U.S. Bureau of Reclamation.
- Wong, I., Dober, M., Olig, S., and Terra, F., 2006, Site-specific seismic hazard evaluation of the Chino Mine Tailing Ponds, New Mexico: unpublished report prepared for Chino Mines Company.
- Wong, I., Olig, S., Dober, M., Silva, W., Wright, D., Thomas, P., Gregor, N., Sanford, A., Lin, K-W., and Love, D., 2004, Earthquake scenario and probabilistic ground shaking hazard maps for the Albuquerque-Belen-Santa Fe, New Mexico corridor: *New Mexico Geology*, v. 26, p. 3-35.
- Wong, I., Terra, F., Olig, S., and Dober, M., 2011, Site-specific seismic hazard evaluation of the Morenci Mine Tailing Dams, Arizona: unpublished report prepared for Freeport-McMoRan Copper & Gold Inc.
- Wong, I., Thomas, P., Olig, S., and Terra, F., 2008, Site-specific probabilistic and deterministic seismic hazard analyses, Sierrita Tailing Dam, Green Valley, Arizona: unpublished report submitted to Phelps Dodge Sierrita Inc.
- Wong, I., Thomas, P., Zachariasen, J., Hansen, L., Terra, F., and Lowenthal-Savy, D., 2009, Site-specific seismic hazard analyses and development of time histories for Perris Dam, California: unpublished report submitted to California Department of Water Resources.
- WGCEP (Working Group on California Earthquake Probabilities), 2008, The Uniform California Earthquake Rupture Forecast, Version 2 (UCERF 2), USGS Open-File Report 2007-1437/CGS Special Report 203/SCEC Contribution #1138, Version 1.0.
- Youngs, R.R. and Coppersmith, K.J., 1985, Implications of fault slip rates and earthquake recurrence models to probabilistic seismic hazard estimates: *Bulletin of the Seismological Society of America*, v. 75, p. 939-964.

Table 1. Fault Source Parameters for Lake Roberts Dam Analysis

FAULT NO. ¹	FAULT NAME	DISTANCE TO DAM ² (km)	RUPTURE MODEL ³	MAXIMUM RUPTURE LENGTH ⁴ (km)	MAXIMUM MAGNITUDE ⁵ (M)	DIP ⁶ (degrees)	APPROXIMATE AGE OF YOUNGEST OFFSET ⁷	PROBABILITY OF ACTIVITY ⁸	RATE OF ACTIVITY ⁹ (mm/yr)	COMMENTS
941	Alma Mesa fault	92	Independent (1.0)	15	6.1 (0.2) 6.4 (0.6) 6.7 (0.2)	45 E (0.2) 60 E (0.6) 75 E (0.2)	< 1.6 Ma	1.0	0.005 (0.5) 0.02 (0.5)	This north-northeast striking normal fault is near the northwestern margin of the Alma basin along the Arizona - New Mexico border (Menges and Pearthree, 1983; Houser, 1994). The Alma Mesa fault is characterized by 10- to 20-m-high fault scarps on deeply dissected Plio-Pleistocene alluvial fan remnants. Our maximum slip rate assumes 20 m of vertical displacement occurred since 1 Ma whereas the minimum rate assumes 10 m occurred since 2 Ma.
2093	Animas Valley faults	103	Independent (1.0)	20	6.3 (0.2) 6.6 (0.6) 6.9 (0.2)	45 W (0.2) 60 W (0.6) 75 W (0.2)	< 15 ka	1.0	0.005 (0.2) 0.02 (0.6) 0.2 (0.2)	These faults extend along the eastern margin of Animas Valley. Preferred slip rate is based on observations of 2 to 3 m scarps on late Pleistocene fans (Machette <i>et al.</i> , 1998).
Not included in USGS database	Big Burro Mountains fault		Independent (1.0)	38	6.6 (0.2) 6.9 (0.6) 7.2 (0.2)	45 W (0.2) 60 W (0.6) 75 W (0.2)	< 1.6 Ma?	0.7	0.001 (0.5) 0.01 (0.5)	This northwest-striking, southwest-dipping, normal fault along the southwest flank of the Big Burro Mountains is not included in the USGS Quaternary Fault and Fold Database, but we include it as a potential fault source based on mapping of potential Quaternary fault scarps by Machette <i>et al.</i> (1986). They estimate tens of meters of slip in Plio-Pleistocene deposits, but little else is known about this poorly understood fault. Based on its poorer geomorphic expression, we assumed a maximum slip rate similar to the preferred rate of the Gold Hill fault zone to the southeast. We assumed 1 to 2 m of slip occurred since ~1 Ma for the minimum rate. We assigned a slightly lower probability of activity of 0.7 because evidence for repeated Quaternary movement is not as strong as other faults in the region that were included by Machette <i>et al.</i> (1998) in their Quaternary fault compilation.
2084	Blue Mountain fault	47	Independent (1.0)	15	6.1 (0.2) 6.3 (0.6) 6.7 (0.2)	45 W (0.2) 60 W (0.6) 75 W (0.2)	< 750 ka	1.0	0.009 (0.2) 0.05 (0.6) 0.1 (0.2)	This northeast-striking normal fault exhibits 330 m of throw in Tertiary volcanic rocks (Elston, 1957) and nearly continuous scarps that are 10 to 15 m high on Quaternary alluvial surfaces (Qp 1) along the southern half of the fault (Seager <i>et al.</i> , 1982). Unfortunately the age of these surfaces are poorly constrained. For our preferred slip rate we assumed they are about 300 ka, whereas for our minimum and maximum we assumed ages of 1.6 Ma and 130 ka, respectively.
2088a and 2088b	Caballo fault	84	Linked (1.0)	21	6.6 (0.2) 6.9 (0.6) ¹⁰ 7.2 (0.2)	45 W (0.2) 60 W (0.6) 75 W (0.2)	< 10 ka	1.0	0.01 (0.2) 0.04 (0.6) 0.5 (0.2)	Source characterization after Wong <i>et al.</i> (1999). We assumed a linked rupture model because the Williamsburg (#2088a) and central (#2088b) sections are continuous along strike, kinematically compatible, individually short for the large displacements per event, and show similar late Quaternary rates of activity (Foley <i>et al.</i> , 1988; Machette <i>et al.</i> , 1998). These faults bound the Caballo Mountains on the west, and together with the Red Hills, Hot Springs, and Derry faults, form the western tectonically active margin of the Caballo uplift. Repeated Pleistocene activity is indicated by 27- to 44-m-high scarps on the Cuchillo surface, the top of the Palomas Formation (estimated to be 700 to 900 ka by Mack <i>et al.</i> , 1993), and trench exposures that reveal evidence for 3 to 4 surface-faulting events since about 150 to 250 ka and average displacements per event of 1.25 to 2 m (Foley <i>et al.</i> , 1988). Our preferred slip rate of 0.04 mm/yr is based on average mid to late Pleistocene rates estimated from scarp studies (Machette, 1987; Foley <i>et al.</i> , 1988) indicating: 3 to 3.7 m surface offsets on 50 to

Table 1. Fault Source Parameters for Lake Roberts Dam Analysis

FAULT NO. ¹	FAULT NAME	DISTANCE TO DAM ² (km)	RUPTURE MODEL ³	MAXIMUM RUPTURE LENGTH ⁴ (km)	MAXIMUM MAGNITUDE ⁵ (M)	DIP ⁶ (degrees)	APPROXIMATE AGE OF YOUNGEST OFFSET ⁷	PROBABILITY OF ACTIVITY ⁸	RATE OF ACTIVITY ⁹ (mm/yr)	COMMENTS
	Caballo fault (<i>continued</i>)									150 ka alluvium; 4.6 to 12.5 m offsets on 150 to 300 ka alluvium; and 5 to 5.5 m offsets on 150 to 300 ka alluvium (expanded age range for the Tortugas Formation reflecting maximum of Machette <i>et al.</i> , 1998 and minimum of Foley <i>et al.</i> , 1988). Minimum slip rate based on a ~145 ky recurrence interval between the pre-Picacho/post-Tortugas event (~150 ka) and the next youngest event (< 5 ka) in Trench 1 of Foley <i>et al.</i> (1988), and assuming a displacement of 2 m for this event. Maximum slip rate was also based on evidence in Trench 1 for possibly two Holocene events occurring between 1.6 and 4 to 5 ka; we assumed a displacement of 1.25 m following a 2400-year interval for this apparently anomalously short seismic cycle.
937	Cactus Flats faults	145	Independent (1.0)	9	5.9 (0.2) 6.2 (0.6) 6.5 (0.2)	50 E (0.2) 65 E (0.6) 80 E (0.2)	< 750 ka	0.9	0.001 (0.3) 0.004 (0.4) 0.04 (0.3)	This northwest-striking series of normal faults and fractures in basin-fill and terrace gravels of the Gila River are located in the hanging wall of the Safford fault zone and are unusually straight. Because of this and their relatively short length (< 10 km), we assigned a slightly lower probably of activity of 0.9 as they may be non-tectonic subsidence features or secondary to the Safford fault zone. We assumed slightly steeper dips than typical range-bounding normal faults because of their intrabasin location and very straight traces (Houser, 1994). Preferred slip rate is based on 0.5 m offset since 130 ka, whereas the maximum rate is based on 100 m of offset of a 2.5-Ma volcanic tuff (Machette <i>et al.</i> , 1986; 1998). The minimum rate assumes 0.5 m of slip occurred since 500 ka.
939, 2090, and 2091	Clifton-Rimrock-Pearson Mesa faults	85	Linked (0.2) Not linked (0.8) Clifton faults Not linked (0.8) (ctd.) Rimrock fault Pearson Mesa faults	36 (floating over total length of 67 km) 31 36 17	6.6 (0.2) 6.9 (0.6) 7.2 (0.2) 6.5 (0.2) 6.8 (0.6) 7.1 (0.2) 6.6 (0.2) 6.9 (0.6) 7.2 (0.2) 6.2 (0.2) 6.5 (0.6) 6.8 (0.2)	45 W (0.2) 60 W (0.6) 75 W (0.2) 70 E (0.3) 90 (0.3) 70 W (0.4)	< 130 ka < 1.6 Ma < 130 ka	1.0	0.005 (0.2) 0.02 (0.6) 0.1 (0.2) 0.003 (0.2) 0.01 (0.6) 0.1 (0.2) 0.005 (0.2) 0.02 (0.6) 0.1 (0.2) 0.003 (0.2) 0.009 (0.6) 0.1 (0.2)	These northwest-striking were considered as potentially linked because they are all down-to-the-southwest normal faults along the northeastern margin of Duncan Basin (Machette <i>et al.</i> , 1998; Pearthree, 1998). Our depiction here includes additional potential Quaternary fault scarps not shown in the USGS database based on mapping by Machette <i>et al.</i> (1986). See text for discussion of maximum magnitudes and rates of activity.
2104	Cuchillo Negro fault zone	73	Independent (1.0)	34	6.6 (0.2) 6.9 (0.6) 7.2 (0.2)	70 E (0.3) 90 (0.3) 70 W (0.4)	< 130 ka	1.0	0.005 (0.2) 0.02 (0.6) 0.2 (0.2)	This broad zone of intrabasin faults has one long prominent trace with scarps 10 to 15 m high and several additional traces with scarps less than 5 m high on the 400 to 900 ka Cuchillo surface (Machette <i>et al.</i> , 1998). Our preferred slip rate assumes 16 m of cumulative slip occurred since 650 ka.

Table 1. Fault Source Parameters for Lake Roberts Dam Analysis

FAULT NO. ¹	FAULT NAME	DISTANCE TO DAM ² (km)	RUPTURE MODEL ³	MAXIMUM RUPTURE LENGTH ⁴ (km)	MAXIMUM MAGNITUDE ⁵ (M)	DIP ⁶ (degrees)	APPROXIMATE AGE OF YOUNGEST OFFSET ⁷	PROBABILITY OF ACTIVITY ⁸	RATE OF ACTIVITY ⁹ (mm/yr)	COMMENTS
2086 and 2089	Derry Hills and Foothills faults	85	Linked (1.0)	14	6.1 (0.2) 6.4 (0.6) 6.7 (0.2)	45 W (0.2) 60 W (0.6) 75 W (0.2)	< 750 ka	1.0	0.003 (0.2) 0.007 (0.6) 0.02 (0.2)	These faults were linked because they form a nearly continuous structure along the southwestern margin of Salem bench, have the same sense of slip, appear to have similar behavior, and are individually too short to be considered as independent sources. Preferred slip rate based on small but multiple event scarps on the Derry Hills fault on deposits that are estimated to be deposited 700 to 900 ka (Machette <i>et al.</i> , 1998). Minimum rate assumes 5 m of Quaternary slip, whereas maximum values assume offsets as large as 2 m could possibly go undetected in late Pleistocene deposits.
2094a and 2094b	Gold Hill fault zone	72	Linked (1.0)	24	6.3 (0.2) 6.7 (0.6) 7.0 (0.2)	45 W (0.2) 60 W (0.6) 75 W (0.2)	< 130 ka	1.0	0.002 (0.2) 0.01 (0.6) 0.09 (0.2)	This normal fault bounds the southwestern flank of the Big Burro Mountains. We assumed a linked rupture model for the northern (2094a) and southern (2094b) sections based on their short individual lengths and kinematic compatibility. Reconnaissance scarp studies found evidence of repeated Quaternary activity with scarps 6 to 8.5 m high on older alluvial fan surfaces (Machette <i>et al.</i> , 1986). Preferred slip rate based on 2.9 m of surface offset measured on surfaces estimated to be 200 to 500 ka (Machete <i>et al.</i> , 1998).
2100 and 2102	Hot Spring and Walnut Springs faults	84	Linked (1.0)	44	6.8 (0.2) 7.1 (0.6) 7.4 (0.2)	45 W (0.2) 60 W (0.6) 75 W (0.2)	< 1.6 Ma	1.0	0.003 (0.2) 0.01 (0.6) 0.045 (0.2)	These normal faults bound the margin between the Engle Basin to the west and the Caballo block to the east. We linked these faults because they overlap considerably and are kinematically compatible with each other, and show similar geomorphic expression and age of activity. However, little is known about either of them. Although the Hot Spring fault offsets 2 to 3 Ma basalts by as much as 90 m (Machette, 1987), it does not appear to offset Rio Grande terrace deposits older than 150 ka (Foley <i>et al.</i> , 1988), suggesting that rates of activity decreased since mid Quaternary time. Significant (but unquantified) offsets of the Palomas Formation also supports early Pleistocene activity along both faults (Machette <i>et al.</i> , 1998). Our maximum rate is based on 90 m of offset since 2 Ma and our preferred rate allows for as much as 2 m of undetected slip since 150 ka, whereas the minimum rate assumes only 2 m of slip occurred since 700 ka.
2137	Mangas fault	37	Independent (1.0)	24	6.4 (0.2) 6.7 (0.6) 7.0 (0.2)	45 SW (0.2) 60 SW (0.6) 75 SW (0.2)	< 1.6 Ma	1.0	0.06 (0.2) 0.01 (0.6) 0.003 (0.2)	The Mangas fault is a northwest-striking, west-dipping normal fault that forms the boundary between the Little Burro Mountains to the northeast and Mangas Valley to the southwest. Based on our observations of possible Quaternary scarps and deformation of older Quaternary alluvium, the fault is assessed to be potentially active and we assign a probability of activity of 1.0. Fault parameters and fault geometry are based on the mapping of Machette <i>et al.</i> (1986). Slip rates are generally based on our scarp height observations and assumed ages, with the preferred value of 0.01 mm/yr based on assuming 13.7 m of vertical slip occurred since the Quaternary (1.6 Ma), and then

Table 1. Fault Source Parameters for Lake Roberts Dam Analysis

FAULT NO. ¹	FAULT NAME	DISTANCE TO DAM ² (km)	RUPTURE MODEL ³	MAXIMUM RUPTURE LENGTH ⁴ (km)	MAXIMUM MAGNITUDE ⁵ (M)	DIP ⁶ (degrees)	APPROXIMATE AGE OF YOUNGEST OFFSET ⁷	PROBABILITY OF ACTIVITY ⁸	RATE OF ACTIVITY ⁹ (mm/yr)	COMMENTS
	Mangas fault (<i>continued</i>)									converting this to dip-slip assuming a 60° dip. The minimum value of 0.003 mm/y is based on assuming 12.2 m of vertical slip occurred since 5 Ma, whereas our maximum value of 0.06 mm/yr assumes 24.4 m of vertical slip occurred since 500 ka. Similarly, these vertical rates were converted to dip-slip rates assuming a 60° fault dip.
2013 and 2012	Mockingbird Hill fault zone and Mogollon fault	31	Linked (1.0)	22	6.3 (0.2) 6.6 (0.6) 6.9 (0.2)	45 W (0.2) 60 W (0.6) 75 W (0.2)	< 750 ka	1.0	0.02 (0.2) 0.08 (0.6) 0.7 (0.2)	These normal faults are assumed to be linked due to their adjacent, nearly continuous, along-strike position, kinematic compatibility along the eastern margin of the Mangas graben, and individual short lengths. Preferred slip rate based on 110 m of offset of Clum Mine pediment gravels, which are believed to be Plio-Pleistocene (assumed ~1.6 Ma).
2101	Mud Springs fault	80	Independent (1.0)	20	6.3 (0.2) 6.6 (0.6) 6.9 (0.2)	45 W (0.2) 60 W (0.6) 75 W (0.2)	< 750 ka	1.0	0.005 (0.2) 0.02 (0.6) 0.2 (0.2)	This normal fault bounds the east side of the Palomas Basin north of the Caballo fault. Little is known about rates of activity except 2 to 10 m high scarps are preserved on the 400 to 900 ka Cuchillo surface (Machette <i>et al.</i> , 1998). Our preferred slip rate assumes 10 m of slip since 650 ka.
2103	Palomas Creek fault zone	65	Independent (1.0)	27	6.4 (0.2) 6.7 (0.6) 7.0 (0.2)	70 E (0.4) 90 (0.3) 70 W (0.3)	< 750 ka	1.0	0.005 (0.2) 0.02 (0.6) 0.2 (0.2)	Preferred slip rate for this fault within the Palomas Basin is assumed similar to the Cuchillo Negro fault zone.
2087a and 2087b	Red Hills fault	85	Linked (1.0)	14	6.1 (0.2) 6.4 (0.6) 6.7 (0.2)	45 W (0.2) 60 W (0.6) 75 W (0.2)	< 130 ka	1.0	0.007 (0.2) 0.03 (0.6) 0.25 (0.2)	This normal fault bounds the eastern margin of Palomas Basin and has significant structural relief. It merges with the Caballo fault to the north and abuts the Derry Hills fault to the south. We assumed the northern (2087a) and southern (2087b) sections of Machette <i>et al.</i> (1998) were linked due to their individual short lengths, continuous along-strike geometry, and kinematic compatibility. We assumed the Red Hills fault behaves independently from the Caballo fault because the former does not appear to have ruptured 1 or 2 times during the Holocene like the Caballo fault. Preferred rate based on 3 to 5 m scarps on late Pleistocene deposits (Machette <i>et al.</i> , 1998).
936a and 936b	Safford fault zone (northern and southern sections)	144	Linked (1.0)	31	6.5 (0.2) 6.8 (0.6) 7.1 (0.2)	45 E (0.2) 60 E (0.6) 75 E (0.2)	< 15 ka	1.0	0.005 (0.2) 0.015 (0.6) 0.1 (0.2)	This northwest-striking, northeast-dipping normal fault extends along the base of the Pinaleno Mountains and is characterized by fault scarps showing recurrent Quaternary movement (Menges and Pearthree, 1983; Machette <i>et al.</i> , 1986). We linked the northern and southern sections because of their individual short lengths, similar scarp morphology and age of youngest movement. Our preferred slip rate is based on 5 to 10 m of vertical displacement on middle and late Quaternary deposits (Machette <i>et al.</i> , 1986) assumed to be ~500 ka. Maximum and minimum rate assumed to be similar to the Rimrock fault (#2090).

Table 1. Fault Source Parameters for Lake Roberts Dam Analysis

FAULT NO. ¹	FAULT NAME	DISTANCE TO DAM ² (km)	RUPTURE MODEL ³	MAXIMUM RUPTURE LENGTH ⁴ (km)	MAXIMUM MAGNITUDE ⁵ (M)	DIP ⁶ (degrees)	APPROXIMATE AGE OF YOUNGEST OFFSET ⁷	PROBABILITY OF ACTIVITY ⁸	RATE OF ACTIVITY ⁹ (mm/yr)	COMMENTS
2081 and 2082	Sierra de la Uvas fault zone and nearby unnamed faults south of Placitas Arroyo	97	Linked (1.0)	18	6.2 (0.2) 6.5 (0.6) 6.8 (0.2)	45 W (0.2) 60 W (0.6) 75 W (0.2)	< 750 ka	1.0	0.0006 (0.2) 0.007 (0.6) 0.08 (0.2)	We grouped these two northeast-trending normal faults that extend along the Sierra de la Uvas, a Tertiary dome, because of their close proximity to each other. They also are subparallel, have a similar sense of slip (down to the northwest), and so are likely associated with each other (Machette <i>et al.</i> , 1998). Little is known about Quaternary slip rates for these structures that appear to predominantly have been active in the Tertiary, but they do have associated, small- (0.5) to moderate- (< 10 m) sized scarps on the Camp Rice Formation (Machette <i>et al.</i> , 1998). We assumed 9 m of vertical slip occurred since 130 ka for our maximum slip rate, 3 m of slip occurred since 500 ka for our preferred slip rate, and 0.5 m of slip occurred since 900 ka for our minimum slip rate.
2131	Unnamed faults along the San Mateo Mountains	97	Independent (1.0)	41	6.7 (0.2) 7.0 (0.6) 7.3 (0.2)	45 W (0.2) 60 W (0.6) 75 W (0.2)	< 750 ka	1.0	0.013 (0.5) 0.006 (0.5)	These north-south-trending, west-facing scarps are somewhat enigmatic as they occur along the eastern margin and on the east-sloping piedmont of the San Mateo Mountains, and thus are not typical basin-range style normal fault scarps (Machette <i>et al.</i> , 1998). However, given their continuity, linear geometry, great length, and geomorphic prominence, we have assumed they are associated with seismogenic normal faults. Little is known about the Quaternary behavior of these faults, but scarps may be as high as 8 m on the 700-900 ka Palomas Formation (Ferguson, 1988). Our maximum rates assumes 8 m of vertical slip occurred since 700 ka, whereas our minimum rate assumes 5 m of slip occurred since 900 ka.
2011	Unnamed faults east of Alma	73	Independent (1.0)	12	6.0 (0.2) 6.3 (0.6) 6.6 (0.2)	55 W (0.2) 70 W (0.6) 85 W (0.2)	< 1.6 Ma	1.0	0.003 (0.5) 0.02 (0.5)	These north-striking normal faults along the western flank of the Mogollon Mountains are characterized by lineaments and possible scarps on high level alluvial surfaces formed on the Plio-Pleistocene basin fill of the Gila Conglomerate (Ratte, 1981). Our maximum rate assumes as much as 10 m of offset occurred since 500 ka, whereas our minimum rate assumes 5 m of offset occurred since 1.6 Ma.
2134	Unnamed faults on the Cuchillo Plain	65	Independent (1.0)	16	6.2 (0.2) 6.5 (0.6) 6.8 (0.2)	45 E (0.2) 60 E (0.6) 75 E (0.2)	< 1.6 Ma	0.5	0.002 (0.2) 0.01 (0.6) 0.09 (0.2)	These faults form the western margin of Palomas Basin but show insignificant net throw and may just be the result of bending at the edge of a half graben that is bounded by the Mud Springs fault to the east (Machette, 1998), and so we assumed a probability of activity of 0.5. Preferred slip rate assumes 5 m of slip since 650 ka based on small scarps on the Cuchillo surface (Machette <i>et al.</i> , 1998).
2105	Unnamed faults west of Caballo Reservoir	68	Independent (1.0)	17	6.2 (0.2) 6.5 (0.6) 6.8 (0.2)	70 E (0.4) 90 (0.3) 70 W (0.3)	< 750 ka	1.0	0.005 (0.2) 0.02 (0.6) 0.2 (0.2)	We assumed steeper dips for this broad zone of faults within the Palomas Basin. Little is known about rates of activity but scarps are similar to those of the Cuchillo Negro fault zone (Machette <i>et al.</i> , 1998) and so we assumed similar rates.

Table 1. Fault Source Parameters for Lake Roberts Dam Analysis

FAULT NO. ¹	FAULT NAME	DISTANCE TO DAM ² (km)	RUPTURE MODEL ³	MAXIMUM RUPTURE LENGTH ⁴ (km)	MAXIMUM MAGNITUDE ⁵ (M)	DIP ⁶ (degrees)	APPROXIMATE AGE OF YOUNGEST OFFSET ⁷	PROBABILITY OF ACTIVITY ⁸	RATE OF ACTIVITY ⁹ (mm/yr)	COMMENTS
2106	Unnamed faults west of Elephant Butte Reservoir	90	Independent (1.0)	16	6.2 (0.2) 6.5 (0.6) 6.8 (0.2)	70 E (0.4) 90 (0.3) 70 W (0.3)	< 750 ka	1.0	0.005 (0.2) 0.02 (0.6) 0.2 (0.2)	Preferred rate assumed similar to the Cuchillo Negro fault zone based on the similarity of scarps (Machette <i>et al.</i> , 1998) for this zone of intrabasin faults.
2097	Unnamed faults west of the Pyramid Mountains	109	Independent (1.0)	16.5	6.2 (0.2) 6.5 (0.6) 6.8 (0.2)	45 W (0.2) 60 W (0.6) 75 W (0.2)	< 130 ka	0.9	0.005 (0.2) 0.02 (0.6) 0.2 (0.2)	These poorly-studied normal faults bound the western flank of the Pyramid Mountains, and are subparallel to the Animas Valley faults (2093), but have more subdued scarps. Based on this and because these faults may be associated with the Animas Valley faults (Machette <i>et al.</i> , 1998), we assumed similar slip rates to the Animas Valley faults, but a slightly lower probability of activity.
2085, 2083, 2099, 2089, and 2139	Zone of faults and folds – southern Caballo uplift (Black Hills, East Rincon Hills, and Central faults; unnamed fold northwest of Rincon, and unnamed fault west of Hatch)	95	Linked (1.0)	14	6.1 (0.2) 6.4 (0.6) 6.7 (0.2)	50 W (0.2) 65 W (0.6) 80 W (0.2)	< 750 ka	1.0	0.01 (0.2) 0.05 (0.6) 0.4 (0.2)	We grouped these short discontinuous faults and folds because they form a broad zone of primarily down to the west deformation at the southern end of the Caballo uplift and they are individually too short to consider as independent sources. All of the faults have scarps that offset the upper section of the Camp Rice Formation, including 10 to 30 m of probable offset along the East Rincon Hills fault (Seager and Hawley, 1973). Our preferred rate is based on 10 to 30 m of offset since 400 to 500 ka.

1. Fault number and nomenclature after Machette *et al.* (1998) and USGS Quaternary Fault and Fold Database of the U.S. unless noted otherwise (<http://earthquakes.usgs.gov/regional/qfaults>).
2. The approximate horizontal distance between the site and the fault trace.
3. Possible rupture models include: zones, independent single faults, segmented and unsegmented faults, and linked faults. Zones are modeled as random point sources within the zone boundary. Segmented and unsegmented faults allow for independent rupture for sections (or segments) of the fault. A linked model allows for coseismic rupture of faults, either along or across strike.
4. Straight-line distance measured end to end on the USGS database unless noted otherwise.
5. Preferred values estimated using the empirical relation of Wells and Coppersmith (1994) for all fault types. Estimates are based on displacement per event and/or maximum surface rupture length, depending on available data.
6. Dips are averages for the seismogenic crust.
7. Based on data in the USGS database. Categories are: Pliocene (1.6 to 5.3 Ma); Quaternary (<1.6 Ma); Pleistocene (10 ka to 1.6 Ma); early Pleistocene (750 ka to 1.6 Ma); late and middle Quaternary (<750 ka); late Quaternary (<130 ka); latest Pleistocene (10 to 15 ka); and Holocene (<10 ka).
8. Probability of activity, p(a), considers the likelihood that a fault is an independent seismogenic structure and is still active within the modern stress field.
9. Rates of fault activity are average net slip rates unless noted otherwise. For most faults, we assumed pure normal slip (100% dip slip) and so these values were calculated from vertical slip rates (typically reported in the literature) by assuming the preferred fault dips. Most of the faults are poorly studied and slip rate data are often lacking. Therefore, unless specified otherwise in the comments column, minimum and maximum slip rates are 5th and 95th percentiles estimated using the approach and weights of Wong *et al.*, 2004). Recurrence models used in the analysis are not explicitly shown for each fault, but included characteristic (weighted 0.6), maximum magnitude (weighted 0.2), and exponential (weighted 0.2).
10. Preferred Mmax based on the average of expected magnitudes estimated from: 2 m of average displacement (yielding **M** 7.2), and 21 km length (yielding **M** 6.6). Magnitudes estimated using Wells and Coppersmith (1994) empirical relations for all fault types.

Table 2a. Southern California and Baja California Fault Source Parameters¹

Fault Name fm2.1 (0.5) ⁷ fm 2.2 (0.5)	P(a) ²	Rupture Length (km)	Slip Rate (mm/yr)	SR unc. ³	Aseismic slip factor ⁴	Paleoseismic Recurrence Interval (yrs)	Sense of Slip ⁵	Downdip Width (km)	Width unc.	Rupture Top (km)	Rupture Bottom (km)	Dip (degrees)	Dip Direction	Preferred Mmax ± 0.3 ⁶
San Andreas Fault Zone [segmented (0.9)]														
San Andreas-1906 rupture	1.0	473.0	24.0	3.0	0.0	300	rl-ss	13.0	2	0	13.0	90		7.9
San Andreas Parkfield	1.0	36.4	34.0	5.0	0.8	24.5	rl-ss	10.2	2	0	10.2	90		6.7
San Andreas-Cholame	1.0	62.5	34.0	5.0	0.0	155	rl-ss	12.0	2	0	12.0	90		7.0
San Andreas-Carrizo	1.0	59.0	34.0	3.0	0.0	175	rl-ss	15.1	2	0	15.1	90		7.1
San Andreas-Big Bend	1.0	49.7	34.0	3.0	0.0	175	rl-ss	15.1	2	0	15.1	90		7.0
San Andreas-Mojave N	1.0	36.9	27.0	7.0	0.0	155	rl-ss	15.1	2	0	15.1	90		6.8
San Andreas-Mojave S	1.0	97.6	29.0	7.0	0.0	130	rl-ss	13.1	2	0	13.1	90		7.3
San Andreas-San Bernardino N	1.0	35.3	22.0	6.0	0.0	175	rl-ss	12.8	2	0	12.8	90		6.8
San Andreas-San Bernardino S	1.0	43.4	16.0	6.0	0.0	200	rl-ss	12.8	2	0	12.8	90		6.9
San Andreas-San Gorgonio Pass/Garnet Hill	1.0	55.9	10.0	6.0	0.0	225	rl-ss	19.3	2	0	16.4	58	N	7.0
San Andreas-Coachella	1.0	69.4	20.0	5.0	0.1	212	rl-ss	11.1	2	0	11.1	90		7.1
Rupture Scenarios (see SoSAF Table 2b)														
San Jacinto - Imperial Fault Zone [segmented (0.9)]														
Imperial	1.0	45.8	20.0	5.0	0.1	—	rl-ss	14.7	2	0	14.6	82	N	6.9
Superstition Hills	1.0	36.2	4.0	2.0	0.1	—	rl-ss	12.6	2	0	12.6	90		6.8
Superstition Mountain	1.0	26.3	5.0	3.0	0.1	395	rl-ss	12.4	2	0	12.4	90		6.6
San Jacinto-Borrego	1.0	34.2	4.0	2.0	0.1	130	rl-ss	13.1	2	0	13.1	90		6.7
San Jacinto-Coyote Creek	1.0	42.9	4.0	2.0	0.0	375	rl-ss	15.9	2	0	15.9	90		6.9
San Jacinto-Clark	1.0	46.8	14.0	6.0	0.0	240	rl-ss	16.8	2	0	16.8	90		7.0
San Jacinto-Anza	1.0	46.1	18.0	6.0	0.0	240	rl-ss	16.8	2	0	16.8	90		7.0
San Jacinto-Anza stepover	1.0	24.2	9.0	4.0	0.0	—	rl-ss	16.8	2	0	16.8	90		6.6
San Jacinto-SJV stepover	1.0	24.2	9.0	4.0	0.0	—	rl-ss	16.8	2	0	16.8	90		6.6
San Jacinto- San Jacinto Valley	1.0	18.5	18.0	6.0	0.0	—	rl-ss	18.5	2	0	18.5	90		6.5
San Jacinto-San Bernardino	1.0	45.1	6.0	4.0	0.0	200	rl-ss	16.1	2	0	16.1	90		6.9
Rupture Scenarios (see Table 2c)														
Elsinore Fault Zone [segmented (0.9)]														
Elsinore-Coyote Mountain	1.0	38.8	3.0	1.0	0.0	933	rl-ss	13.3	2	0	13.2	82	NE	6.8
Elsinore-Julian	1.0	75.4	3.0	1.0	0.0	2000	rl-ss	18.9	2	0	18.8	84	NE	7.3
Elsinore-Temecula	1.0	40.0	5.0	2.0	0.0	600	rl-ss	14.2	2	0	14.2	88	NE	6.8
Elsinore-Temecula stepover	1.0	11.8	2.5	2.0	0.0		rl-ss	13.5	2	0	13.3	80	NE	6.3
Elsinore-Glen Ivy stepover	1.0	11.8	2.5	2.0	0.0		rl-ss	13.5	2	0	13.3	80	SW	6.3
Elsinore-Glen Ivy	1.0	25.8	5.0	2.0	0.0	271	rl-ss	13.5	2	0	13.3	80	SW	6.6
Elsinore-Whittier (fm2.1) (0.5)	1.0	46.2	2.5	1.0	0.0	—	rl-ss	14.6	2	0	14.1	75	NE	6.9

Table 2a. Southern California and Baja California Fault Source Parameters¹

Fault Name	P(a) ²	Rupture Length	Slip Rate	SR unc. ³	Aseismic slip factor ⁴	Paleoseismic Recurrence Interval	Sense of Slip ⁵	Downdip Width	Width unc.	Rupture Top (km)	Rupture Bottom (km)	Dip	Dip Direction	Preferred Mmax ± 0.3 ⁶
Elsinore-Whittier (fm2.2) (0.5)	1.0	46.2	2.5	1.0	0.0	—	rl-ss	13.2	2	0	12.4	70	NE	6.9
Rupture Scenarios (see Elsinore Table 1e)						—								
Earthquake Valley ⁷	1.0	20.4	2.0	1.0	0.0	—	rl-ss	18.8	2	0	18.8	90		6.6
Laguna Salada	1.0	99.5	3.5	1.5	0.0	—	rl-ss	13.3	2	0	13.3	90		7.3
SHEAR ZONES														
Eastern CA Shear zone	0.5	219.0	4.0	2.0	0.0	—	rl-ss	14.0	2	0	14.0	90		7.6

¹ Parameters are discussed in more detail in Wong *et al.* (2009) and are largely after the 2007 California Geological Survey/U.S. Geological Survey Uniform California Earthquake Rupture Forecast (UCERF) model (WGCEP, 2008).

² Probability of activity

³ Uncertainty in slip rate value. Single number implies slip rates are modeled with slip rate value in “Slip Rate” column ± value in “SR unc.”, with weightings of 0.2, 0.6, 0.2.

⁴ Aseismic slip factor (ASF) is used to account for some fraction of aseismic slip due to fault creep by decreasing the effective coseismic rupture area (multiply fault area by 1-ASF to determine effective rupture area). A totally locked fault will have an ASF of 0 and a fully creeping fault will have an ASF of 1.0.

⁵ (ss) strike slip, (r) reverse, (n) normal, (rl) rt. lateral, (ll) left lateral, (o) oblique

⁶ Mmax obtained either from historical data or calculated from empirical magnitude-area (M-A) and/or magnitude-length (M-L) relationships. For strike-slip faults we used the average of Wells and Coppersmith (1994) M-L and Hanks and Bakun (2002) M-A relationships; for others, we used the average of Wells and Coppersmith (1994) M-L and M-A relationships.

⁷ “fm2.1” and “fm2.2” refer to two alternative fault models used in the calculations, weighted equally. Refer to WGCEP (2008) for discussion.

⁸ Earthquake Valley fault: not modeled as separate source for sites far from fault. Rather it is included in Elsinore calculations (Julian and Coyote Mtn segments).

⁹ Values shown in this cell are not uncertainties in slip rate as described in note 2, but weights on the corresponding slip rates in the “Slip Rate” column.

Table 2b. Maximum Magnitudes and Rupture Rates for the Southern San Andreas Fault

	Rupture Name (segments involved)	Area (km²)	Ells-B Mag	H&B Mag	A-Priori Rate	Ells-B Rate	H&B Rate	Comments
	Weight				0.5	0.25	0.25	
1	PK	78	6.09	5.87	3.46E-02	2.49E-02	5.26E-02	Rupture area is reduced from fault by 0.79 aseismic factor
2	CH	750.2	7.08	6.9	5.00E-05	5.21E-05	5.46E-05	
3	CC	891.2	7.15	7	3.00E-04	1.60E-04	5.74E-05	
4	BB	751	7.08	6.9	3.00E-04	5.68E-04	5.26E-04	
5	NM	556.5	6.95	6.73	2.00E-04	1.05E-04	1.44E-04	
6	SM	1279	7.31	7.21	5.00E-04	6.45E-04	6.78E-04	
7	NSB	451.9	6.86	6.64	7.00E-04	7.12E-04	6.64E-04	
8	SSB	555.5	6.94	6.73	5.00E-05	5.10E-05	5.17E-05	
9	BG	843	7.13	6.97	5.00E-04	1.88E-04	1.35E-05	
10	CO	693.4	7.04	6.86	2.50E-03	6.70E-03	1.21E-02	Rupture area is reduced from fault by 0.1 aseismic factor
11	PK+CH	828.2	7.12	6.96	1.60E-03	4.36E-03	7.01E-03	
12	CH+CC	1641.4	7.42	7.36	3.00E-04	2.39E-04	2.15E-04	
13	CC+BB	1642.2	7.42	7.36	0	5.02E-06	5.07E-06	
14	BB+NM	1307.5	7.32	7.23	0	1.01E-06	1.01E-06	
15	NM+SM	1835.4	7.46	7.42	7.00E-04	4.95E-06	5.04E-06	
16	SM+NSB	1730.9	7.44	7.39	6.00E-04	8.79E-04	8.90E-04	
17	NSB+SSB	1007.4	7.2	7.07	8.00E-04	1.05E-03	1.22E-03	
18	SSB+BG	1398.5	7.35	7.26	9.00E-04	5.03E-06	4.95E-06	
19	BG+CO	1536.4	7.39	7.32	7.00E-04	2.83E-04	4.10E-04	
20	PK+CH+CC	1719.4	7.44	7.38	7.00E-04	4.26E-04	4.19E-04	
21	CH+CC+BB	2392.4	7.58	7.58	0	9.94E-07	9.93E-07	
22	CC+BB+NM	2198.7	7.54	7.53	0	1.00E-06	1.01E-06	
23	BB+NM+SM	2586.4	7.61	7.62	2.50E-04	1.88E-04	2.67E-04	
24	NM+SM+NSB	2287.4	7.56	7.55	1.00E-04	7.24E-05	6.69E-05	
25	SM+NSB+SSB	2286.4	7.56	7.55	4.00E-04	6.05E-04	7.55E-04	
26	NSB+SSB+BG	1850.4	7.47	7.43	4.00E-04	2.22E-04	3.05E-05	
27	SSB+BG+CO	2091.9	7.52	7.5	4.00E-04	2.23E-04	2.48E-04	
28	PK+CH+CC+BB	2470.4	7.59	7.59	4.00E-04	8.20E-04	8.34E-04	
29	CH+CC+BB+NM	2948.8	7.67	7.7	0	9.91E-07	9.99E-07	
30	CC+BB+NM+SM	3477.7	7.74	7.79	4.00E-04	1.95E-04	4.99E-06	
31	BB+NM+SM+NSB	3038.4	7.68	7.71	0	9.95E-07	1.00E-06	
32	NM+SM+NSB+SSB	2842.9	7.65	7.68	2.00E-04	1.04E-04	1.02E-04	
33	SM+NSB+SSB+BG	3129.4	7.7	7.73	3.00E-04	2.92E-04	1.97E-04	
34	NSB+SSB+BG+CO	2543.8	7.61	7.61	4.00E-04	2.23E-04	2.17E-04	
35	PK+CH+CC+BB+NM	3026.9	7.68	7.71	7.00E-04	1.54E-03	1.66E-03	
36	CH+CC+BB+NM+SM	4227.8	7.83	7.9	5.00E-04	4.16E-04	2.67E-04	
37	CC+BB+NM+SM+NSB	3929.6	7.79	7.86	1.00E-04	8.64E-05	5.55E-05	

(from Table 3, Appendix G, WGCEP, 2008)

Table 2b. Maximum Magnitudes and Rupture Rates for the Southern San Andreas Fault

	Rupture Name (segments involved)	Area (km²)	Ells-B Mag	H&B Mag	A-Priori Rate	Ells-B Rate	H&B Rate	Comments
	Weight				0.5	0.25	0.25	
38	BB+NM+SM+NSB+SSB	3593.9	7.76	7.81	5.00E-05	4.92E-05	5.42E-05	
39	NM+SM+NSB+SSB+BG	3685.9	7.77	7.83	1.00E-04	6.19E-05	3.29E-05	
40	SM+NSB+SSB+BG+CO	3822.8	7.78	7.85	4.00E-04	3.58E-04	4.16E-04	
41	PK+CH+CC+BB+NM+SM	4305.9	7.83	7.92	2.00E-03	1.04E-03	6.43E-04	
42	CH+CC+BB+NM+SM+NSB	4679.8	7.87	7.96	0	9.91E-07	9.89E-07	
43	CC+BB+NM+SM+NSB+SSB	4485.1	7.85	7.94	1.00E-04	9.04E-05	6.76E-05	
44	BB+NM+SM+NSB+SSB+BG	4436.9	7.85	7.93	0	1.01E-06	1.01E-06	
45	NM+SM+NSB+SSB+BG+CO	4379.2	7.84	7.93	1.00E-04	6.01E-05	3.90E-05	
46	PK+CH+CC+BB+NM+SM+NSB	4757.8	7.88	7.97	5.00E-04	4.21E-04	3.49E-04	
47	CH+CC+BB+NM+SM+NSB+SSB	5235.3	7.92	8.03	5.00E-05	5.00E-05	5.09E-05	
48	CC+BB+NM+SM+NSB+SSB+BG	5328.1	7.93	8.04	5.00E-05	4.44E-05	3.00E-05	
49	BB+NM+SM+NSB+SSB+BG+CO	5130.2	7.91	8.02	5.00E-05	4.50E-05	4.70E-05	
50	PK+CH+CC+BB+NM+SM+NSB+SSB	5313.3	7.93	8.04	1.00E-04	1.00E-04	1.09E-04	
51	CH+CC+BB+NM+SM+NSB+SSB+BG	6078.2	7.98	8.12	0	9.95E-07	1.01E-06	
52	CC+BB+NM+SM+NSB+SSB+BG+CO	6021.5	7.98	8.11	1.00E-05	9.66E-06	9.24E-06	
53	PK+CH+CC+BB+NM+SM+NSB+SSB+BG	6156.3	7.99	8.12	5.00E-05	4.65E-05	4.09E-05	
54	CH+CC+BB+NM+SM+NSB+SSB+BG+CO	6771.6	8.03	8.18	0	1.01E-06	9.93E-07	
55	PK+CH+CC+BB+NM+SM+NSB+SSB+BG+CO	6849.7	8.04	8.18	1.00E-04	8.29E-05	6.59E-05	
<i>Total</i>					<i>5.42E-02</i>	<i>4.88E-02</i>	<i>8.37E-02</i>	

- PK Parkfield
- CH Cholame
- CC Carrizo
- BB Big Bend
- NM Mojave North
- SM Mojave South
- NSB San Bernardino North
- SSB San Bernardino South
- BG San Gorgonio Pass-Garnet Hill (aka Banning-Garnet Hill)
- CO Coachella

(from Table 3, Appendix G, WGCEP, 2008)

Table 2c. Maximum Magnitudes and Rupture Rates for the San Jacinto Fault

	Rupture Name (segments involved)	Area (km²)	Ells-B Mag	H&B Mag	A-Priori Rate	Ells-B Rate	H&B Rate	Comments
	Weight				0.5	0.25	0.25	
1	SBV	725.7	7.06	6.88	2.31E-03	4.39E-04	4.42E-04	
2	SJV (SJV+SJV stepover sections)	686.7	7.04	6.85	2.43E-03	4.50E-04	4.49E-04	
3	A (A+A stepover sections)	1193.9	7.28	7.17	0	8.83E-05	8.82E-05	
4	C	786.1	7.1	6.93	0	8.87E-05	8.98E-05	
5	CC	681.5	7.03	6.85	8.89E-04	4.50E-04	4.48E-04	
6	B	403.6	6.81	6.59	4.82E-03	4.45E-04	4.43E-04	Rupture area is reduced from fault by 0.1 aseismic factor
7	SM	325.8	6.71	6.49	1.09E-03	1.50E-03	4.01E-03	Rupture area is reduced from fault by 0.1 aseismic factor
8	SBV+SJV	1412.4	7.35	7.27	1.32E-03	4.49E-04	4.41E-04	
9	SJV+A	1880.6	7.47	7.44	0	4.41E-04	4.50E-04	
10	A+C	1980.1	7.5	7.47	3.15E-03	1.21E-03	1.16E-03	
11	A+CC	1875.4	7.47	7.43	0	8.82E-05	9.00E-05	
12	CC+B	1085.1	7.24	7.12	8.89E-04	4.50E-04	4.47E-04	
13	B+SM	729.4	7.06	6.89	1.09E-03	4.40E-04	4.43E-04	
14	SBV+SJV+A	2606.4	7.62	7.62	0	4.47E-04	4.48E-04	
15	SJV+A+C	2666.8	7.63	7.64	0	4.48E-04	4.51E-04	
16	SJV+A+CC	2562.2	7.61	7.61	0	8.91E-05	8.93E-05	
17	A+CC+B	2279.1	7.56	7.55	0	9.02E-05	8.95E-05	
18	CC+B+SM	1411	7.35	7.27	8.89E-04	4.48E-04	4.40E-04	
19	SBV+SJV+A+C	3392.5	7.73	7.78	1.05E-03	4.49E-04	4.41E-04	
20	SBV+SJV+A+CC	3287.9	7.72	7.76	0	8.94E-05	9.03E-05	
21	SJV+A+CC+B	2965.8	7.67	7.7	0	8.82E-05	8.89E-05	
22	A+CC+B+SM	2604.9	7.62	7.62	0	8.93E-05	8.96E-05	
23	SBV+SJV+A+CC+B	3691.5	7.77	7.83	0	8.80E-05	8.97E-05	
24	SJV+A+CC+B+SM	3291.6	7.72	7.76	0	8.94E-05	9.03E-05	
25	SBV+SJV+A+CC+B+SM	4017.3	7.8	7.88	0	8.90E-05	8.82E-05	
	<i>Total</i>				<i>1.99E-02</i>	<i>9.04E-03</i>	<i>1.15E-02</i>	

SBV San Bernardino Valley

SJV San Jacinto Valley

A Anza

C Clark

CC Coyote Creek

B Borrego Mountain

SM Superstition Mountain

Note: Does not include Imperial or Superstition Hills faults

(from Table 3, Appendix G, WGCEP, 2008)

Table 2d. Maximum Magnitudes and Rupture Rates for the Elsinore Fault

	Rupture Name (segments involved)	Area (km²)	Ells-B Mag	H&B Mag	A-Priori Rate	Ells-B Rate	H&B Rate	E/HB ave Mag	Comments
	Weight				0.5	0.25	0.25		
1	W	674.8	7.03	6.84	7.14E-04	9.27E-04	1.37E-03	6.94	
2	GI (GI+GI stepover sections)	488.6	6.89	6.67	2.55E-03	1.19E-03	2.19E-03	6.78	
3	T (T+T stepover sections)	734.9	7.07	6.89	6.10E-04	1.24E-04	3.46E-04	6.98	
4	J	1426.1	7.35	7.28	0	3.85E-05	2.48E-05	7.32	
5	CM	517.3	6.91	6.69	5.71E-04	1.04E-03	2.11E-03	6.80	
6	W+GI	1163.4	7.27	7.16	0	2.48E-05	1.42E-04	7.22	
7	GI+T	1223.5	7.29	7.19	8.90E-04	1.25E-04	1.25E-04	7.24	
8	T+J	2161	7.53	7.52	0	1.27E-04	1.26E-04	7.53	
9	J+CM	1943.3	7.49	7.45	0	1.74E-04	2.92E-04	7.47	
10	W+GI+T	1898.3	7.48	7.44	0	2.48E-05	9.07E-05	7.46	
11	GI+T+J	2649.6	7.62	7.63	0	1.26E-04	1.27E-04	7.63	
12	T+J+CM	2678.2	7.63	7.64	2.50E-04	2.83E-04	2.54E-04	7.64	
13	W+GI+T+J	3324.4	7.72	7.77	0	2.52E-05	2.48E-05	7.75	
14	GI+T+J+CM	3166.9	7.7	7.74	2.50E-04	1.83E-04	1.27E-04	7.72	
15	W+GI+T+J+CM	3841.7	7.78	7.85	0	2.49E-05	2.52E-05	7.82	
<i>Total</i>					<i>5.84E-03</i>	<i>4.44E-03</i>	<i>7.37E-03</i>		

- W Whittier
- GI Glen Ivy
- T Temecula
- J Julian
- CM Coyote Mountain

Note: Does not include Laguna Salada fault

(from Table 3, Appendix G, WGCEP, 2008)

Table 3

UHS

Period (sec)	2,475-yr UHS	5,000-yr UHS	10,000-yr UHS
0.01	0.093	0.125	0.163
0.03	0.101	0.136	0.177
0.05	0.121	0.165	0.216
0.1	0.186	0.253	0.334
0.15	0.223	0.305	0.396
0.2	0.225	0.305	0.395
0.3	0.188	0.252	0.328
0.4	0.149	0.204	0.264
0.5	0.121	0.161	0.212
0.75	0.091	0.116	0.146
1.0	0.069	0.088	0.110
1.5	0.043	0.056	0.069
2.0	0.028	0.038	0.050
3.0	0.017	0.021	0.026
4.0	0.012	0.015	0.018
5.0	0.011	0.012	0.015
7.5	0.007	0.009	0.011
10.0	0.005	0.006	0.008

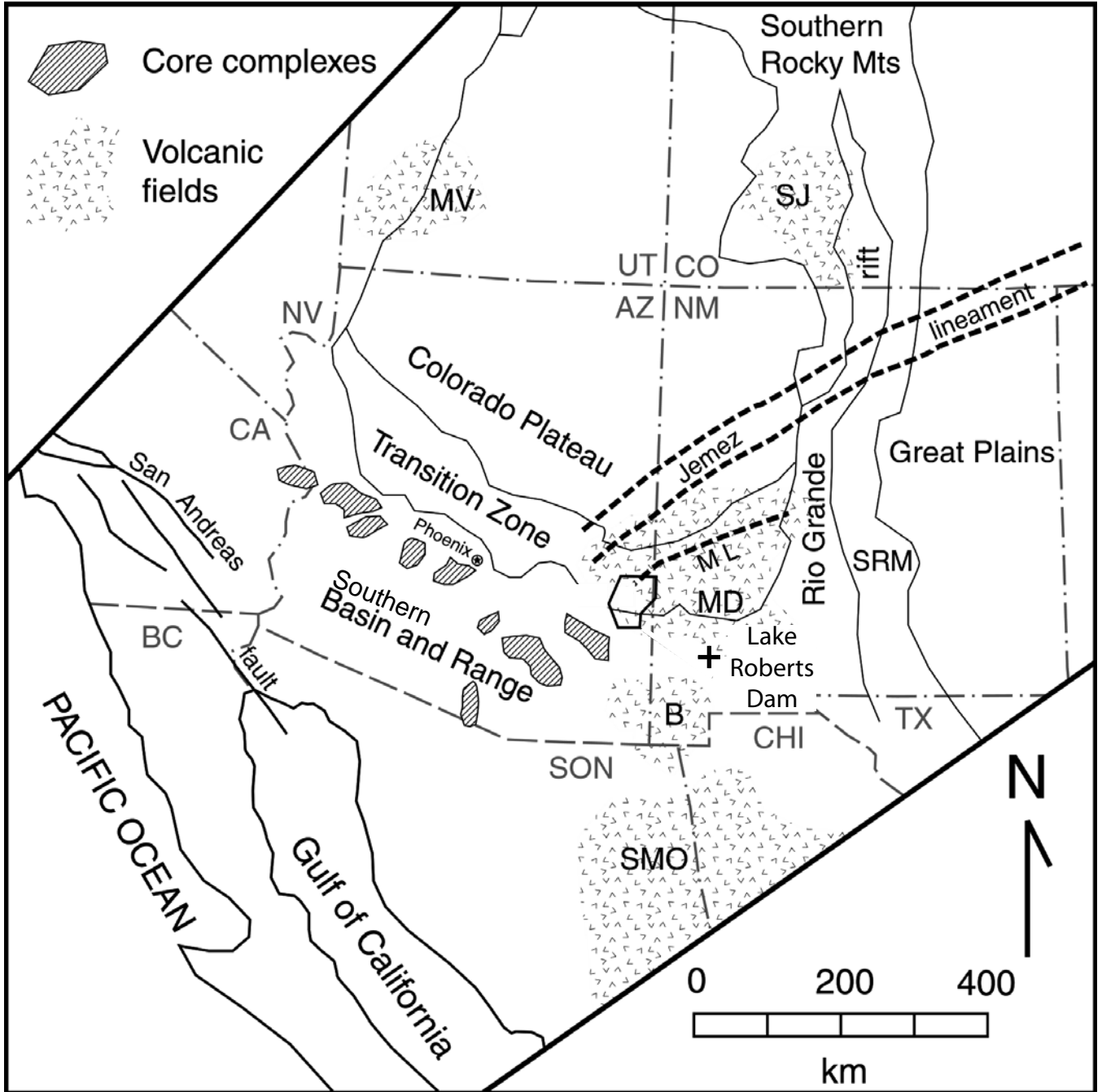
Note: Envelope of V_{s30}

Table 4
PSHA Deaggregation
(V_{s30} of 800 m/sec)

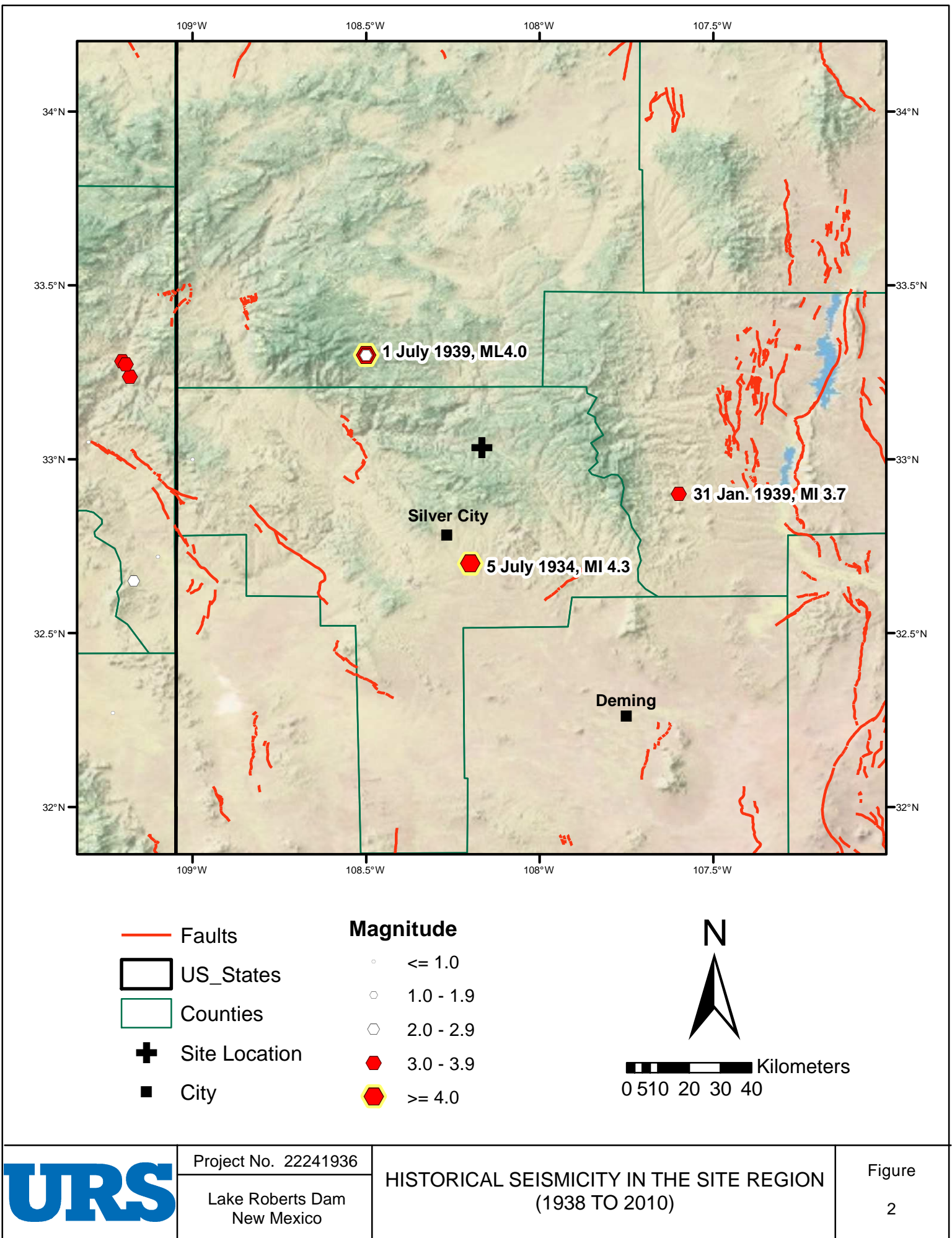
	2475-yr UHS	5000-yr UHS	10000-yr UHS
PGA			
M*	6.45	6.55	6.65
D* (km)	30	30	30
E*	1.1	1.1	1.5
1.0 Sec SA			
M*	6.45	6.55	6.55
D*	35	35	35
E*	1.1	1.3	1.7

Table 5
DSHA Results
(Envelope of V_s30)

Period (sec)	Mockingbird Hill/Mogollon Fault M 6.9 Rrup=31.0 km
0.01	0.138
0.02	0.141
0.03	0.150
0.05	0.177
0.075	0.223
0.1	0.267
0.15	0.325
0.2	0.339
0.25	0.317
0.3	0.293
0.4	0.251
0.5	0.212
0.75	0.145
1.0	0.110
1.5	0.071
2.0	0.050
3.0	0.029
4.0	0.021
5.0	0.017



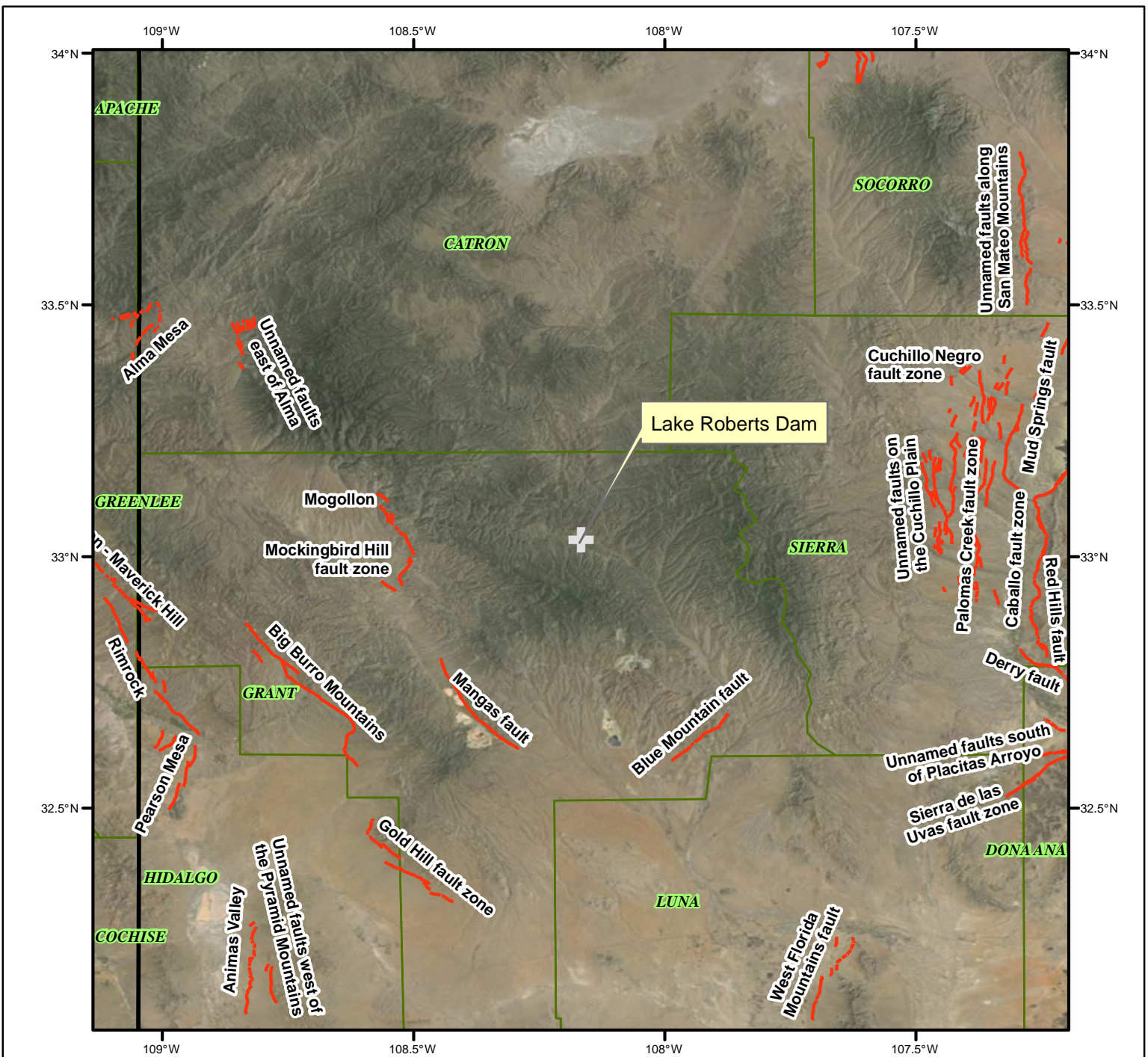
Source: Drewes *et al.* (1985)







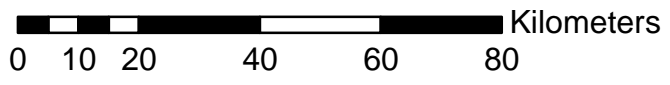
Project No. 22241936
 Lake Roberts Dam
 New Mexico

**HISTORICAL SEISMICITY IN THE SITE REGION
 (1938 TO 2010)**

Figure
 2



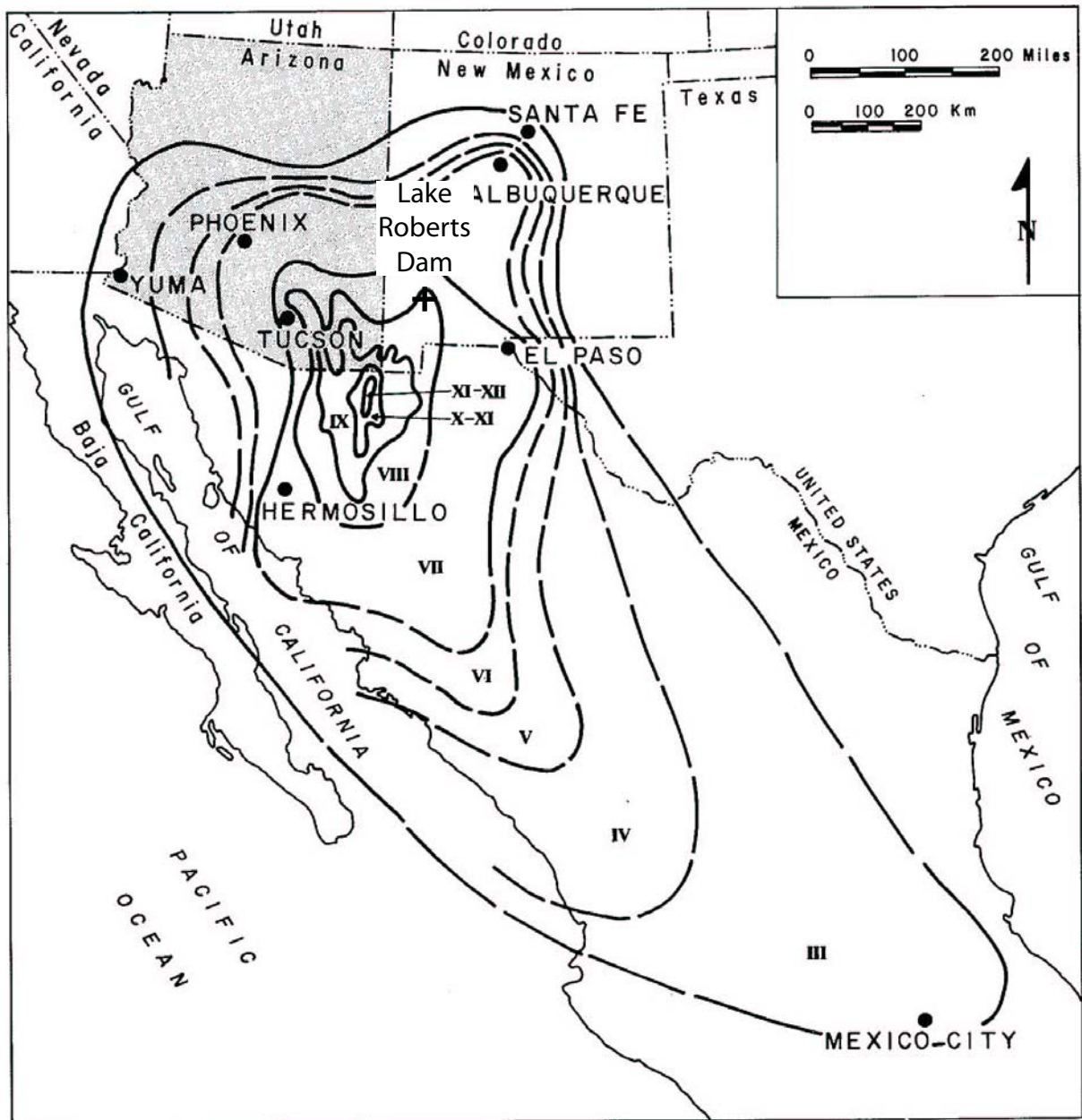
-  Site Location
-  Fault
-  US States
-  Counties



Project No. 22241934
 Lake Roberts Dam
 New Mexico

QUATERNARY FAULTS IN THE SITE REGION

Figure
 3



Modified From DuBois et al., 1982



Project NO. 22241934

Lake Roberts Dam
New Mexico

ISOSEISMAL MAP OF 3 MAY 1887
M 7.4 SONORA, MEXICO EARTHQUAKE

Figure
4

SEISMIC SOURCES

ATTENUATION RELATIONSHIPS

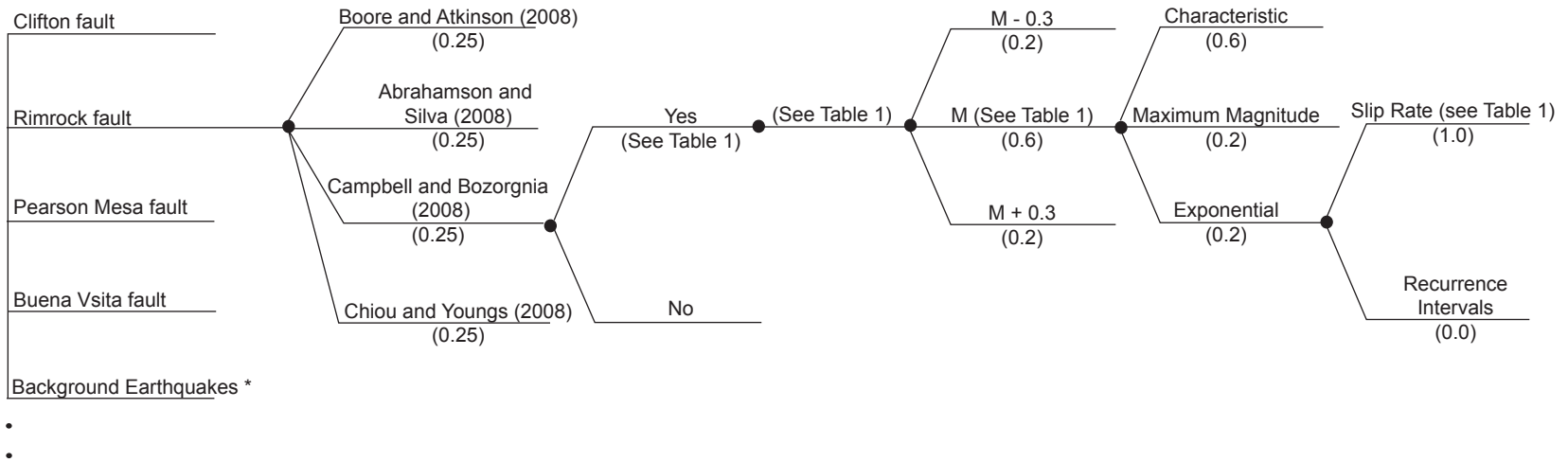
ACTIVITY

SOURCE GEOMETRY
(Dip, Closest Distance, Depth)

MAXIMUM MAGNITUDE

EARTHQUAKE RECURRENCE MODEL

RATE OF ACTIVITY



*Treated as areal source zone and with Gaussian Smoothing, each weighted 50 percent.

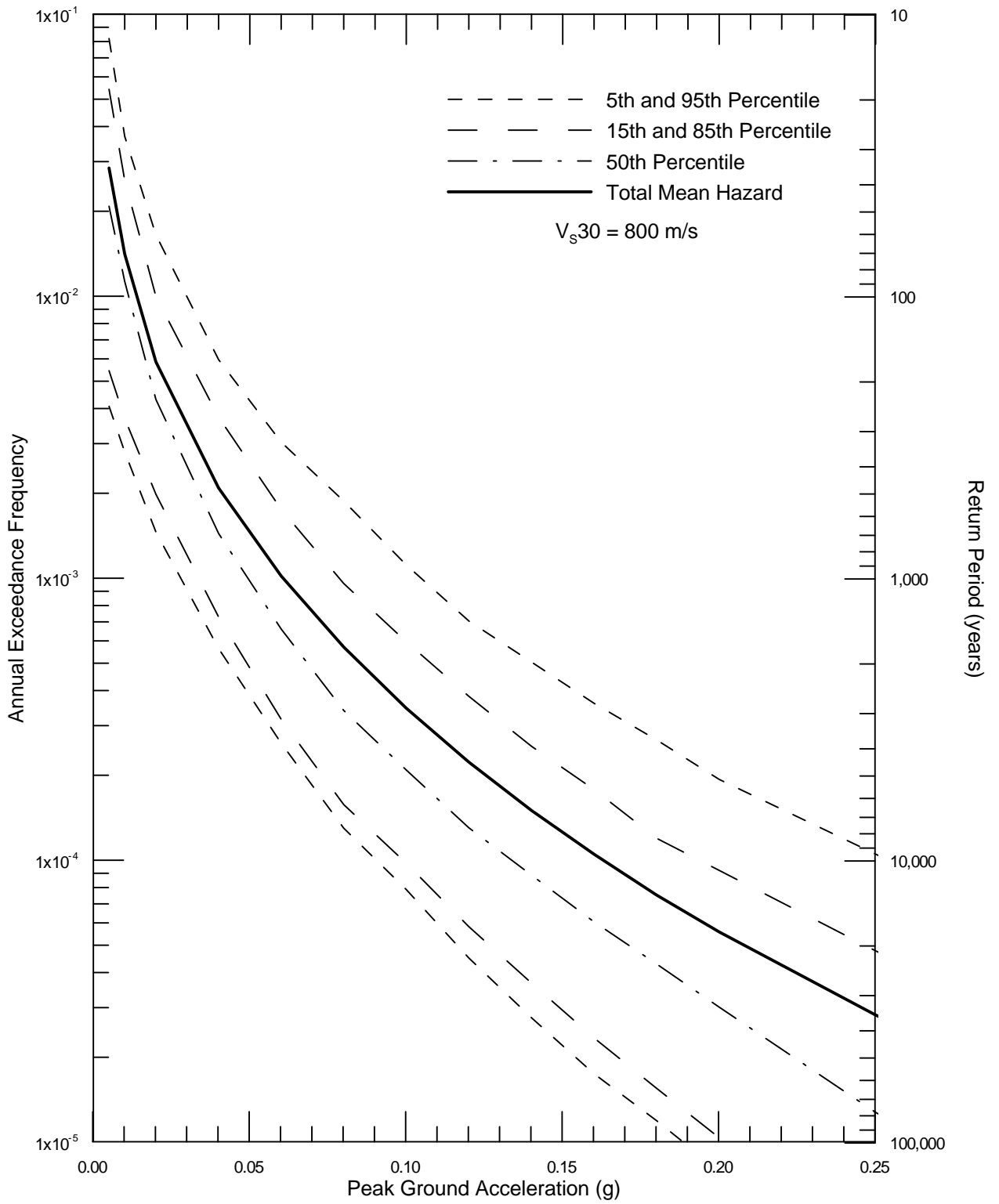


Project NO. 22241931

Ša^ÄÜ[à^:ö Äœ
p^, Ä^c&[

SEISMIC HAZARD
MODEL LOGIC TREE

Figure
5

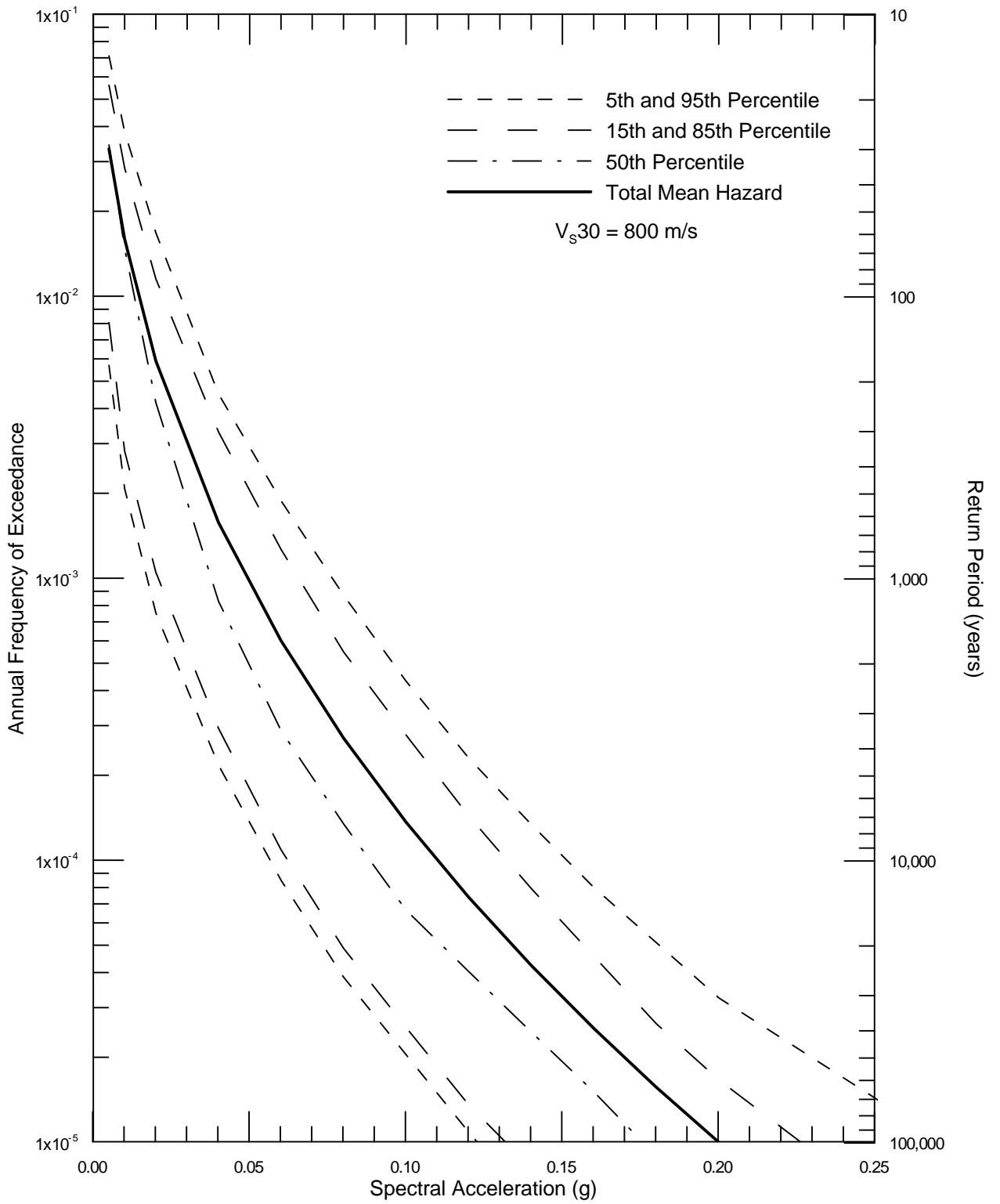


Project No. 22241934

Lake Roberts Dam
New Mexico

SEISMIC HAZARD CURVES FOR
PEAK HORIZONTAL ACCELERATION

Figure
6

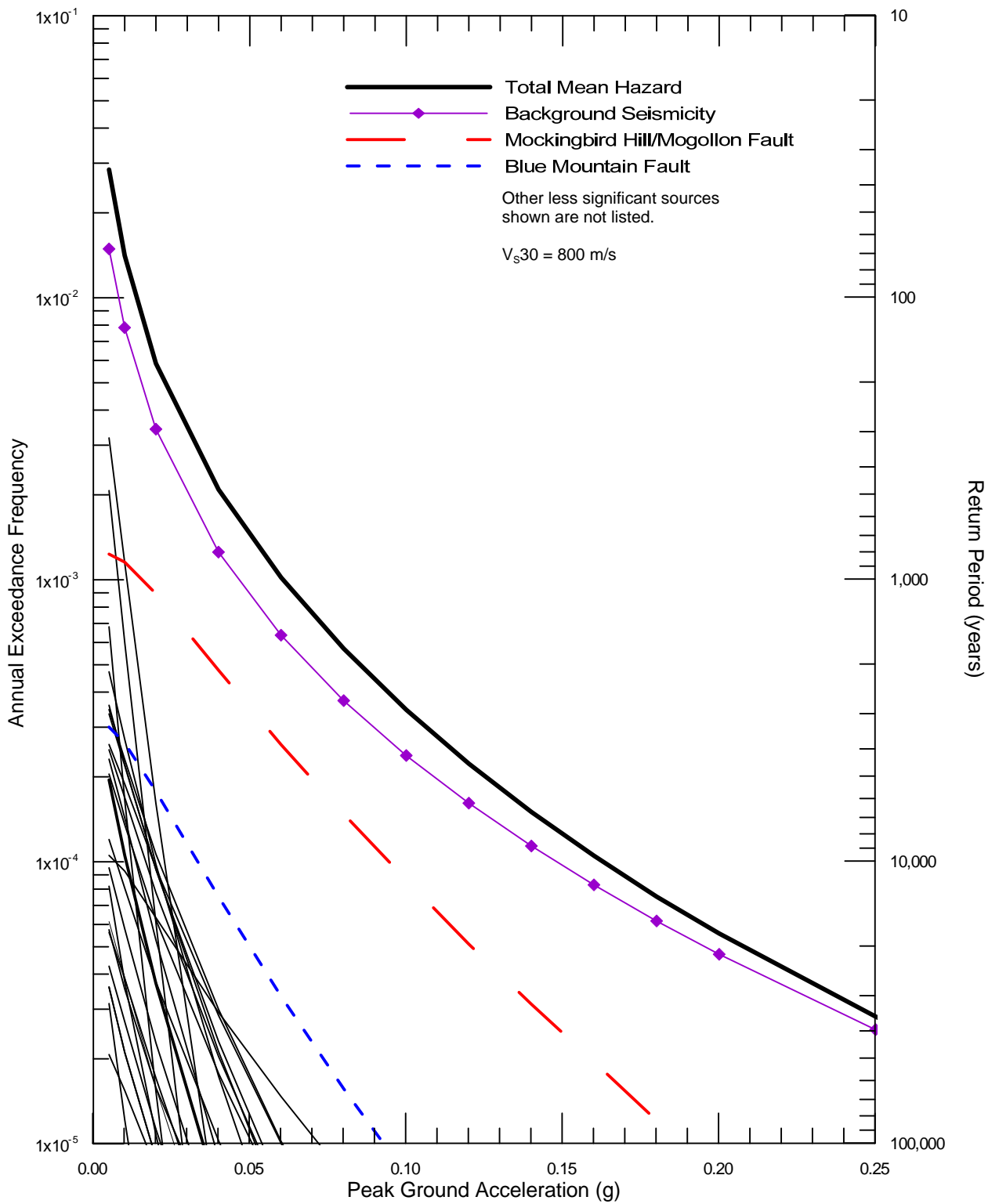


Project No. 22241934

Lake Roberts Dam
New Mexico

SEISMIC HAZARD CURVES FOR 1.0 SEC
HORIZONTAL SPECTRAL ACCELERATION

Figure
7

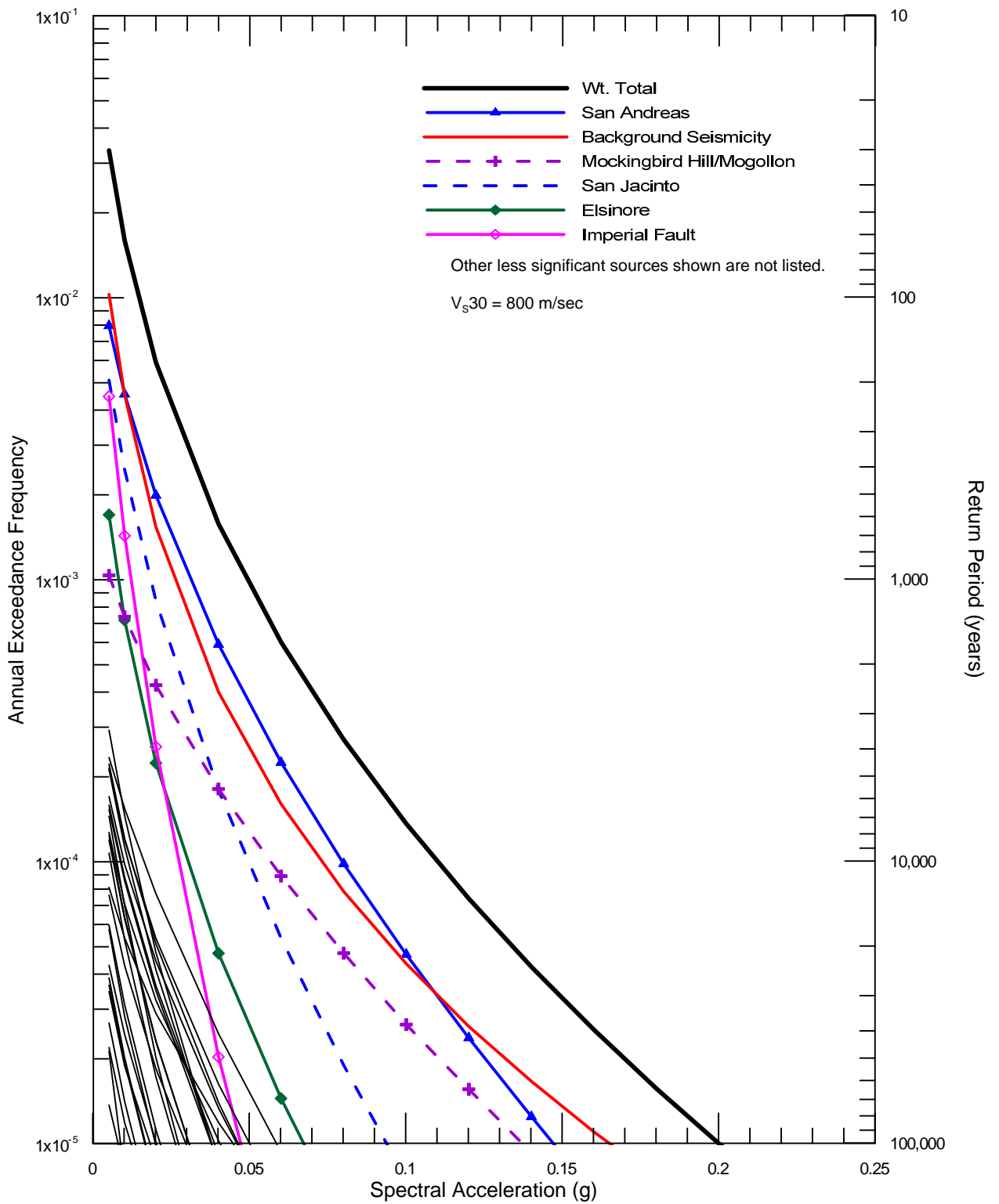


Project No. 22241934

Lake Roberts Dam
New Mexico

SEISMIC SOURCE CONTRIBUTIONS TO MEAN
PEAK HORIZONTAL ACCELERATION HAZARD

Figure
8

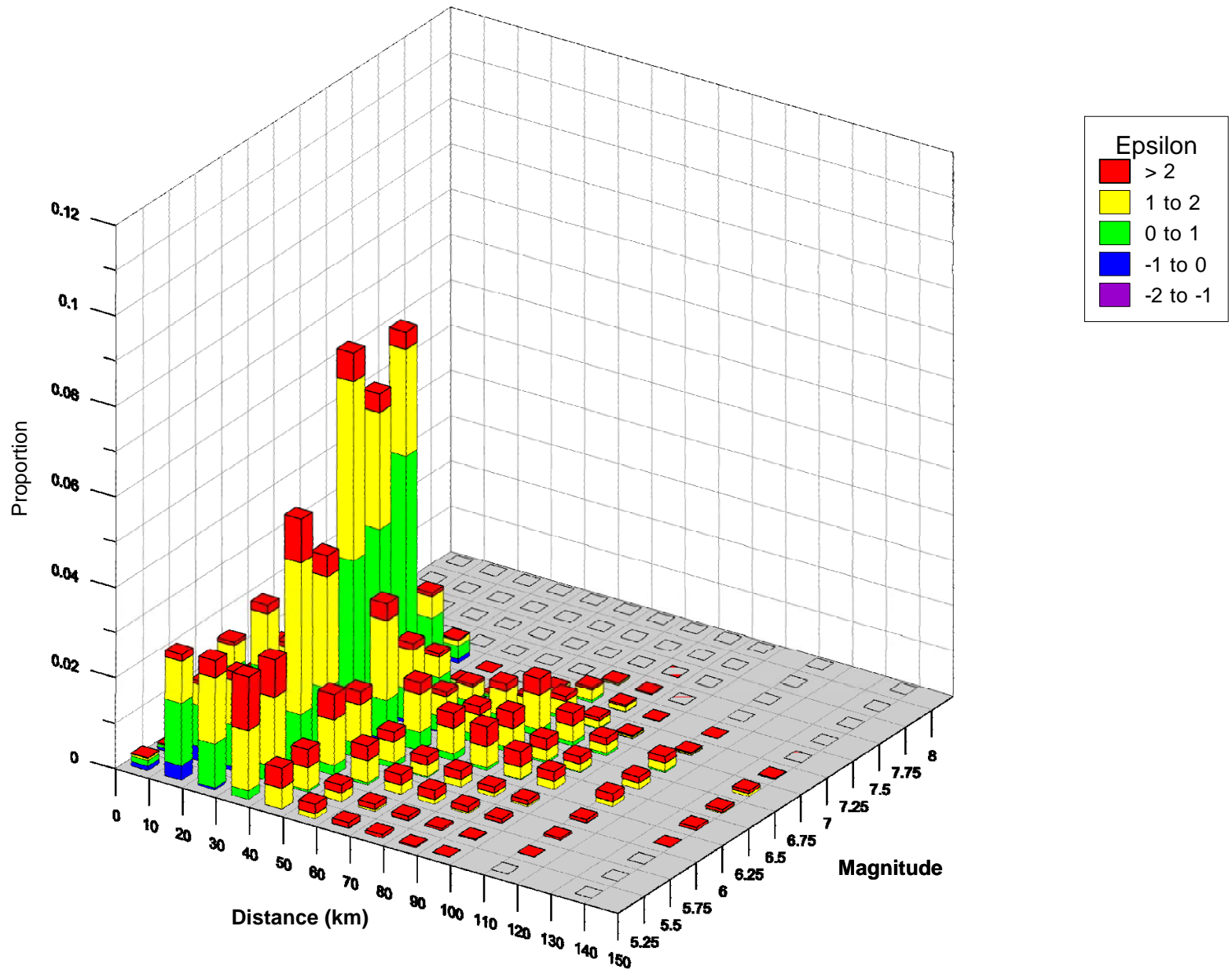


Project No. 22241934

Lake Roberts Dam
New Mexico

SEISMIC SOURCE CONTRIBUTIONS TO MEAN
1.0 SECOND HORIZONTAL SPECTRAL
ACCELERATION HAZARD

Figure
9



$V_{S30} = 800 \text{ m/sec}$

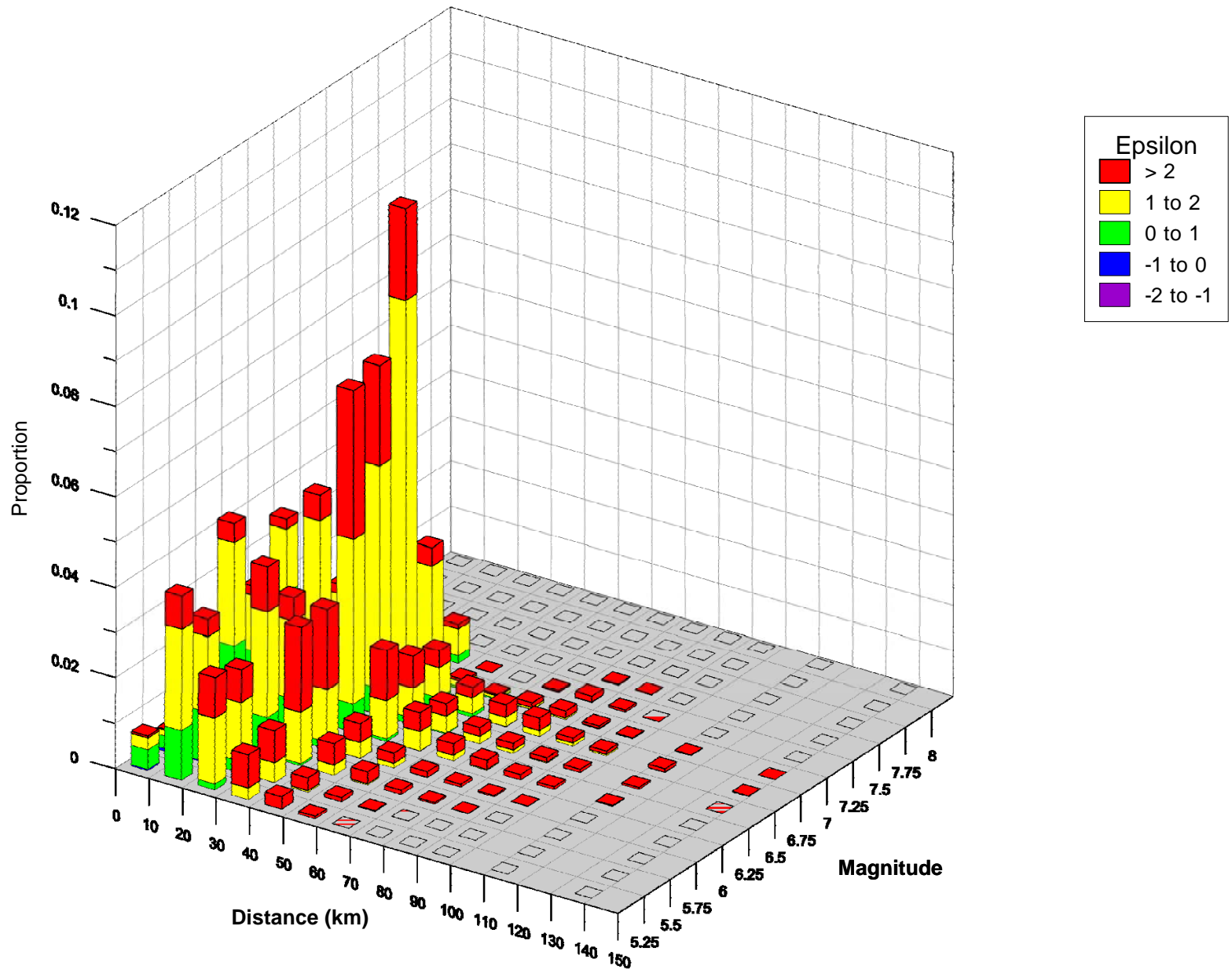


Project No. 22241934

Lake Roberts Dam
New Mexico

MAGNITUDE AND DISTANCE CONTRIBUTIONS
TO THE MEAN PEAK HORIZONTAL ACCELERATION
HAZARD AT 2,475-YEAR RETURN PERIOD

Figure
10



$V_{s30} = 800 \text{ m/sec}$

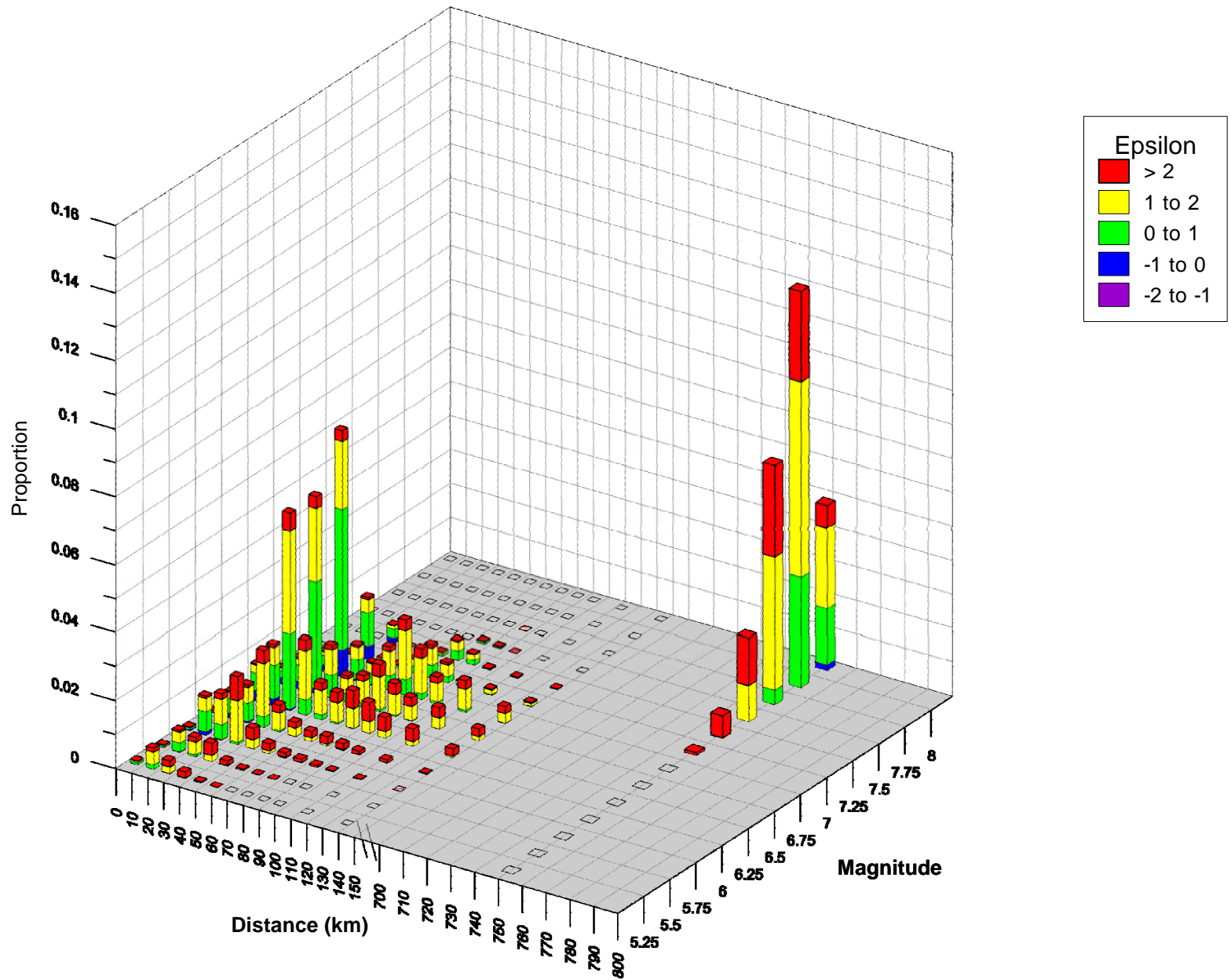


Project No. 22241934

Lake Roberts Dam
New Mexico

MAGNITUDE AND DISTANCE CONTRIBUTIONS
TO THE MEAN PEAK HORIZONTAL ACCELERATION
HAZARD AT 10,000-YEAR RETURN PERIOD

Figure
11



$V_{s30} = 800 \text{ m/sec}$

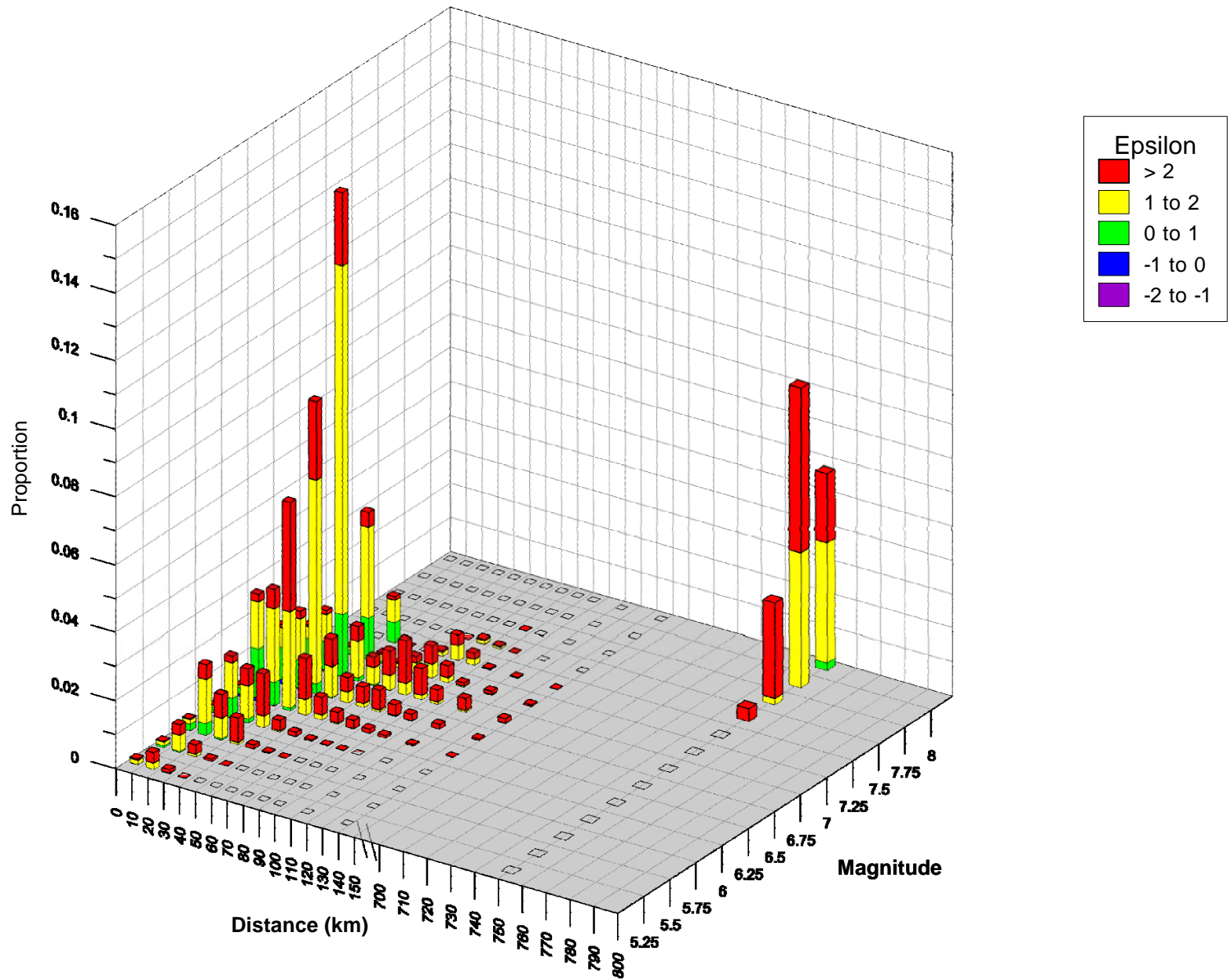


Project No. 22241934

LakeRoberts Dam
New Mexico

MAGNITUDE AND DISTANCE CONTRIBUTIONS
TO THE MEAN 1.0 SEC HORIZONTAL SPECTRAL
ACCELERATIONHAZARD AT
2,475-YEAR RETURN PERIOD

Figure
12



$V_{S30} = 800 \text{ m/sec}$

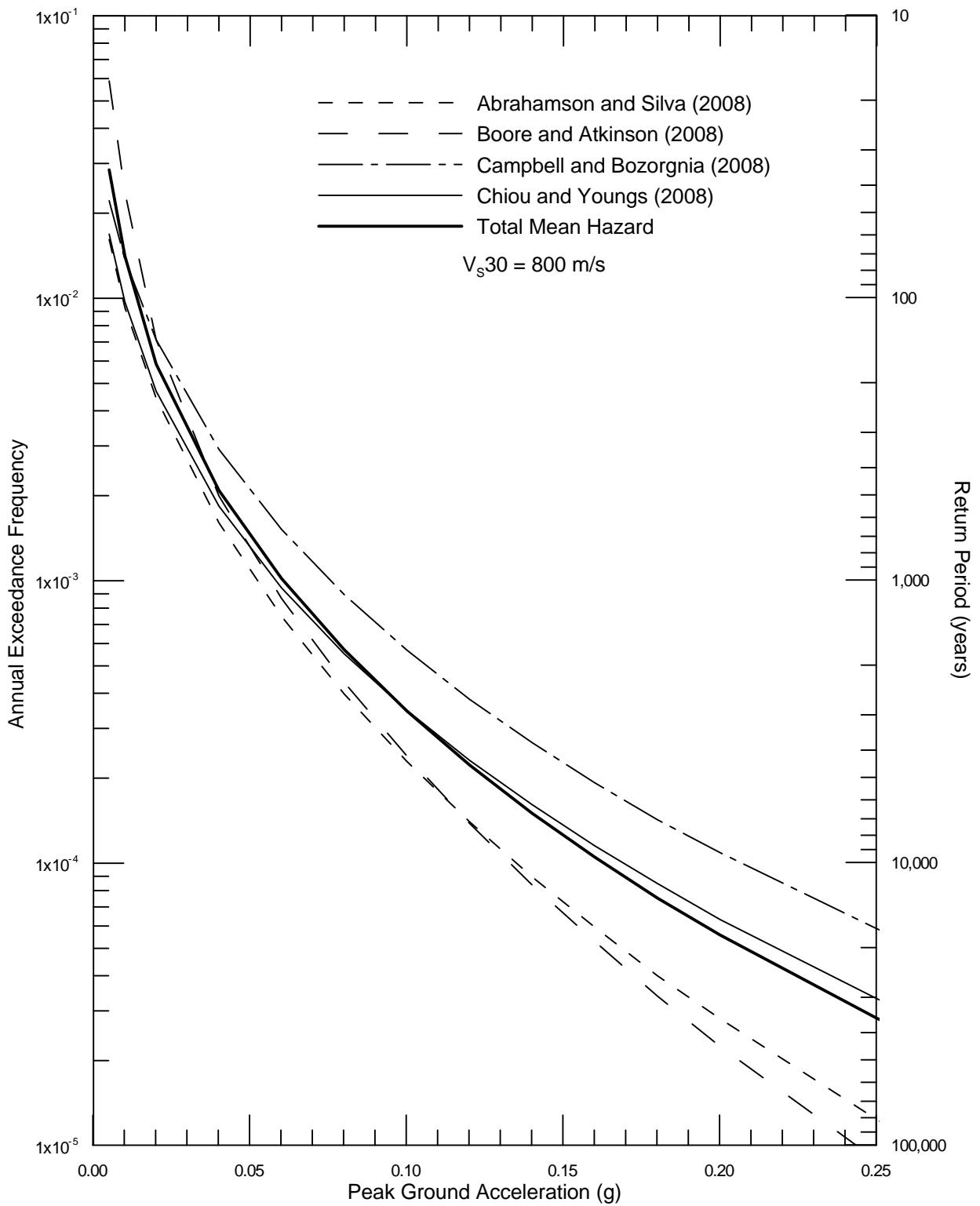


Project No. 22241934

LakeRoberts Dam
New Mexico

MAGNITUDE AND DISTANCE CONTRIBUTIONS
TO THE MEAN 1.0 SEC HORIZONTAL SPECTRAL
ACCELERATION HAZARD AT
10,000-YEAR RETURN PERIOD

Figure
13

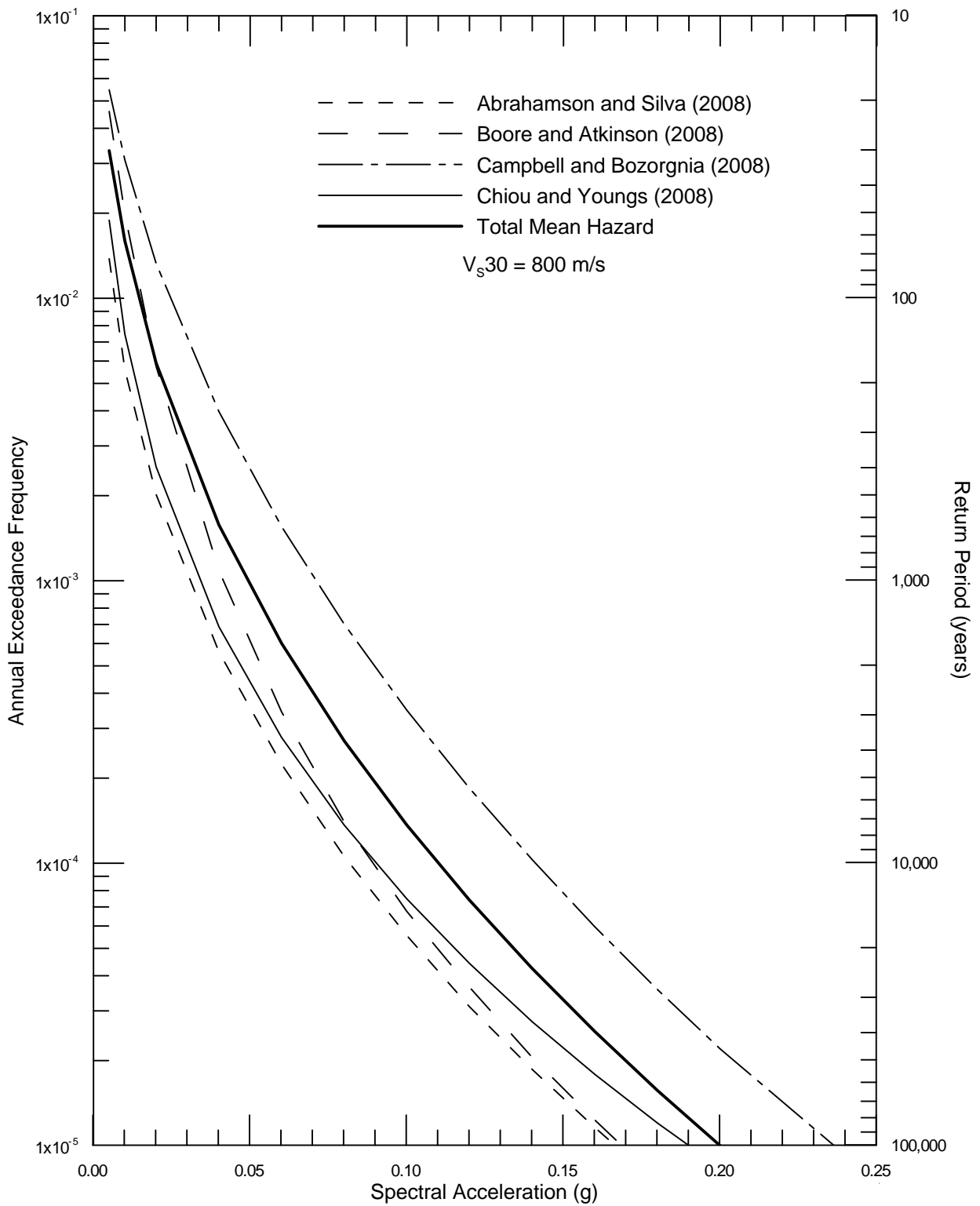


Project No. 22241934

Lake Roberts Dam
New Mexico

SENSITIVITY OF THE PEAK HORIZONTAL
ACCELERATION HAZARD TO THE SELECTION OF
GROUND MOTION PREDICTION MODELS

Figure
14

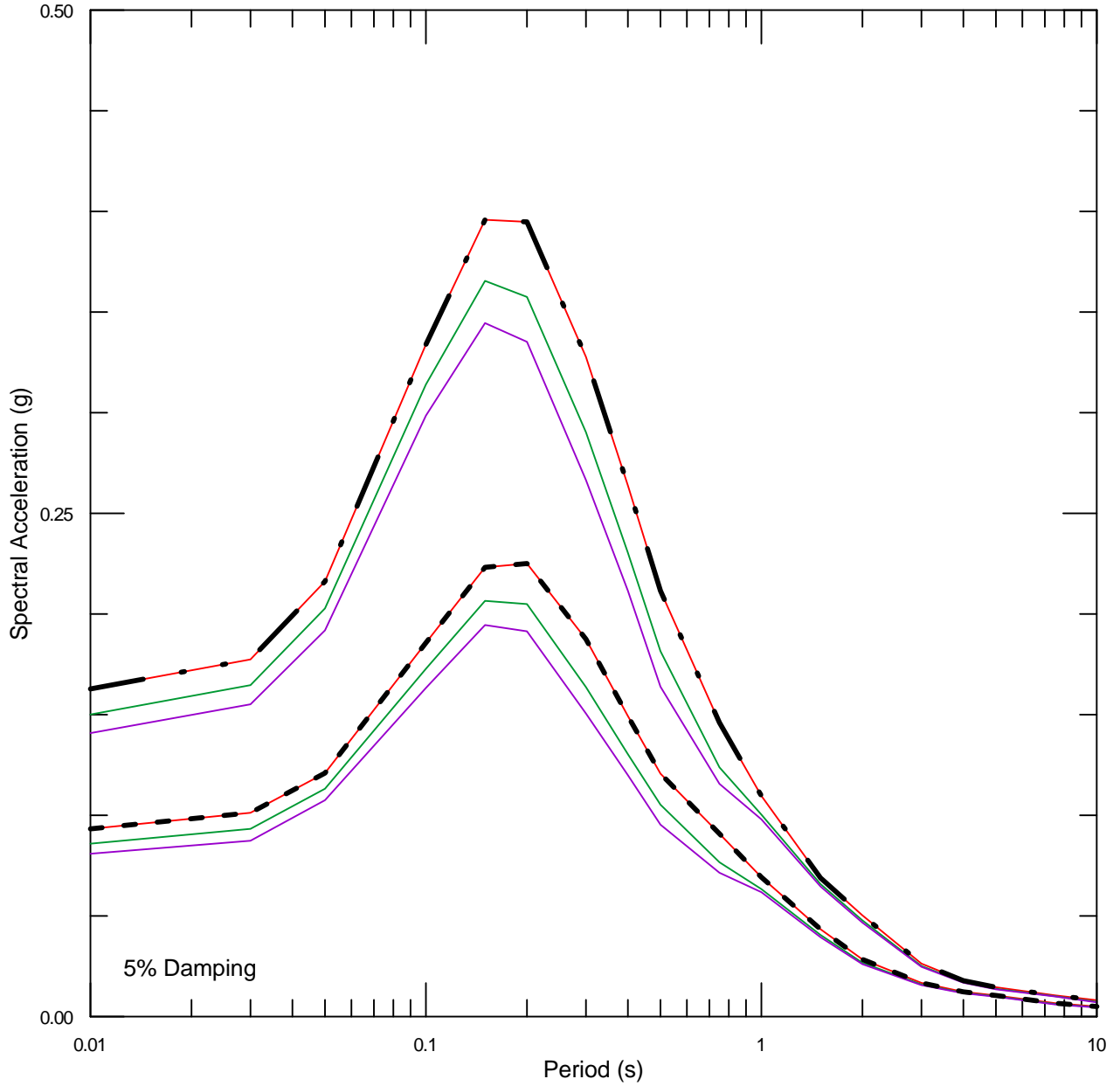


Project No. 22241934

Lake Roberts Dam
New Mexico

SENSITIVITY OF THE 1.0 SEC HORIZONTAL
SPECTRAL ACCELERATION HAZARD TO
THE SELECTION OF GROUND MOTION
PREDICTION MODELS

Figure
15



UHS: Envelope of Vs30 Spectra

- - - - - 2,475-Year Return Period
- . - . - 10,000-Year Return Period

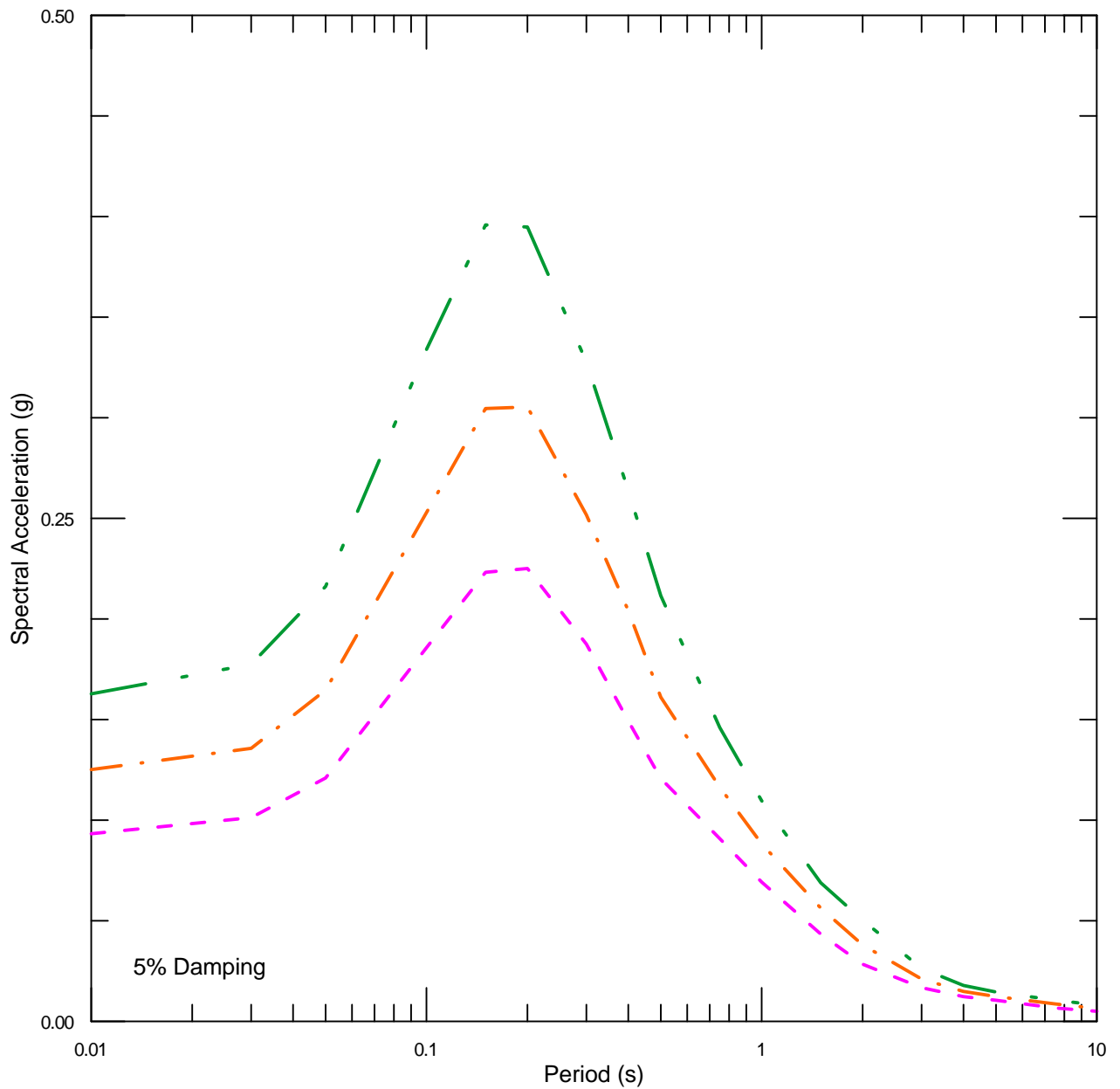
- VS30 = 800 m/sec
- VS30 = 1,000 m/sec
- VS30 = 1,200 m/sec



Project No. 22241934
 Lake Roberts Dam
 New Mexico

5%-DAMPED UNIFORM HAZARD SPECTRA
 AT 2,475 AND 10,000-YEAR RETURN PERIODS

Figure
 16



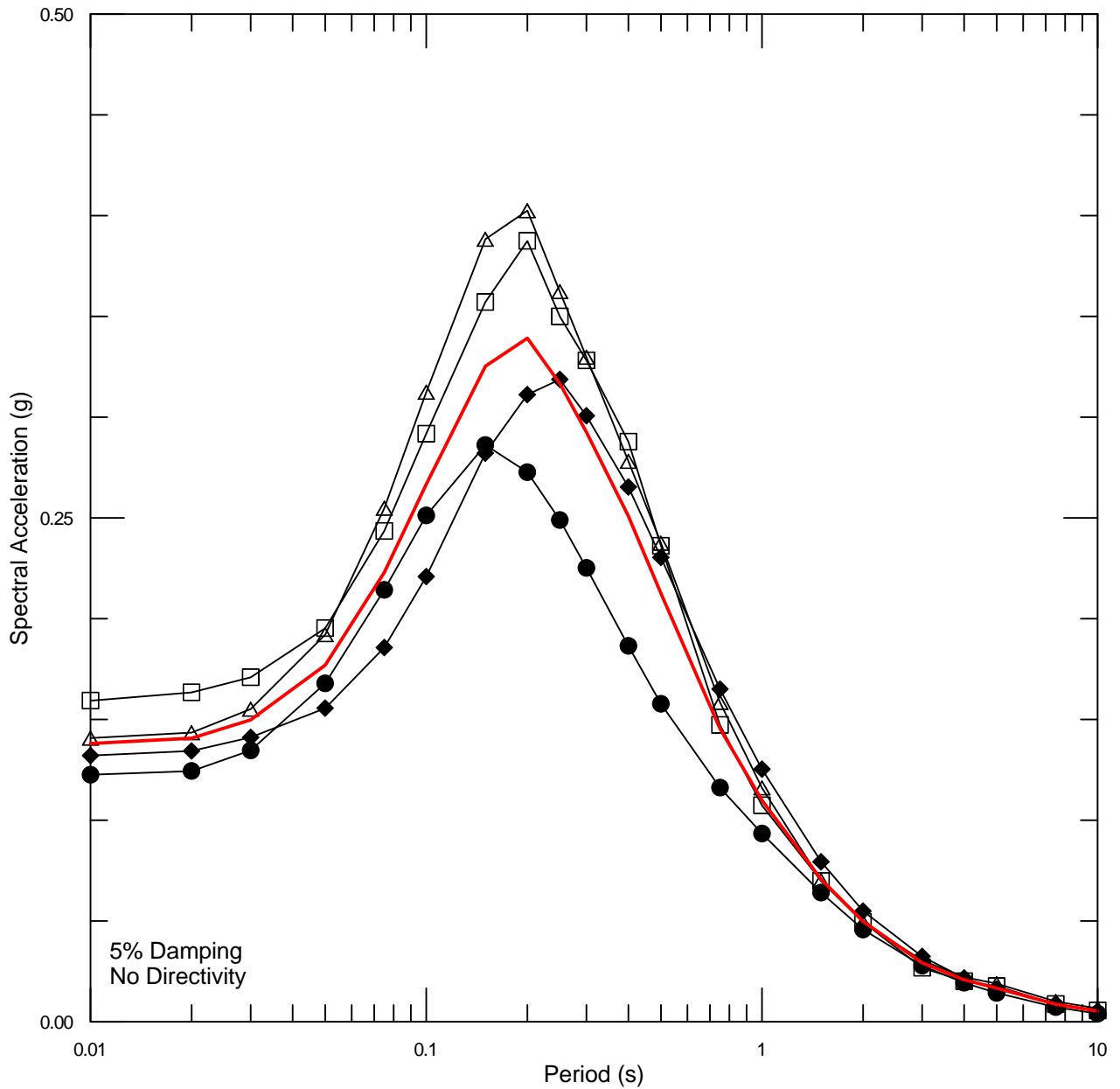
- 2,475-Year Return Period
- . - . 5,000-Year Return Period
- . - . - . 10,000-Year Return Period



Project No. 22241934
 Lake Roberts Dam
 New Mexico

ENVELOPED 5%-DAMPED UNIFORM HAZARD
 SPECTRA AT 2,475, 5,000 AND
 10,000-YEAR RETURN PERIODS

Figure
 17



- ◆— Abrahamson and Silva (2008)
- Boore and Atkinson (2008)
- △— Campbell and Bozorgnia (2008)
- Chiou and Youngs (2008)
- — Lognormal Average

Distances

r_{rup} (rupture) = 31.0 km
 r_x (horizontal) = 31.0 km
 Rupture Width = 17.3 km

Site Condition

V_{s30} = 800 m/sec
 $Z_{1.0}$ = 0.03 km (AS 2008); 0.02 km (CY 2008)
 $Z_{2.5}$ = 0.60 km (CB 2008)

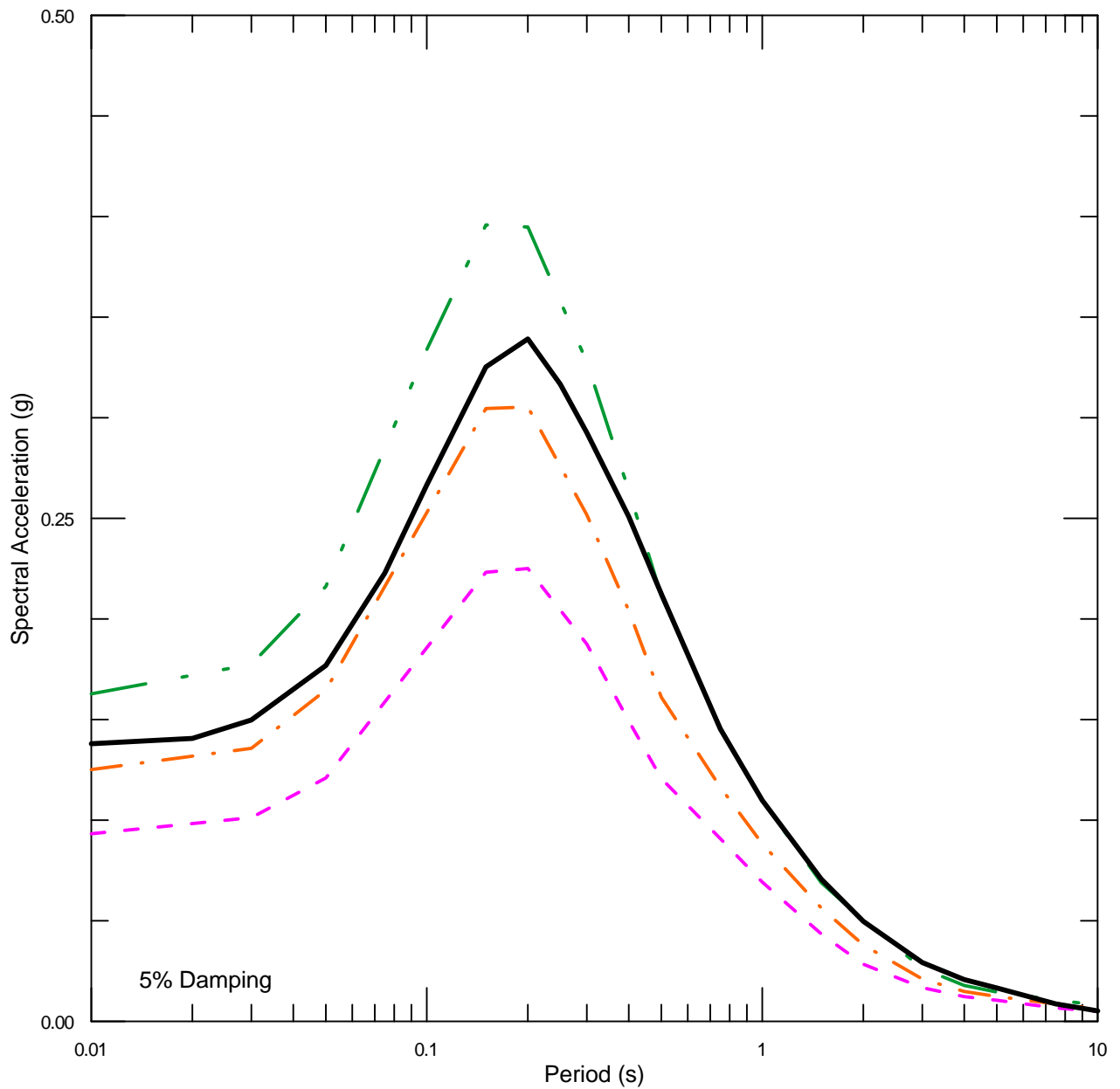
PGA = 0.14 g



Project No. 22241934
 Lake Roberts Dam
 New Mexico

84TH PERCENTILE HORIZONTAL ACCELERATION
 RESPONSE SPECTRA FOR THE M 6.9
 MOCKINGBIRD HILL/MOGOLLON FAULT
 MAXIMUM EARTHQUAKE

Figure
 18



UNIFORM HAZARD SPECTRA

- 2,475-Year Return Period
- .- 5,000-Year Return Period
- .- 10,000-Year Return Period
- 84th Percentile Deterministic
Mockingbird Hill/Mogollon Fault, **M6.9** $R_{RUP} = 31.0$ km



Project No. 22241934
Lake Roberts Dam
New Mexico

ENVELOPED 5%-DAMPED UNIFORM HAZARD
SPECTRA COMPARED TO 84TH PERCENTILE
DETERMINISTIC SPECTRA FOR MOCKINGBIRD
HILL / MOGOLLON FAULT

Figure
19